Limited reversal of regional climate signals in overshoot scenarios

Authors:

Peter Pfleiderer
Hamburg University, Climate Analytics
peter.pfleiderer@climateanalytics

Carl-Friedrich Schleussner
Climate Analytics, Humboldt University Berlin
carl.schleussner@climateanalytics.org

Jana Sillmann
Hamburg University, CICERO
jana.sillmann@uni-hamburg.de

Limited reversal of regional climate signals in overshoot scenarios

Peter Pfleiderer (1,2), Carl-Friedrich Schleussner (2,3), Jana Sillmann (1,4)

1 Universität Hamburg, Germany
2 Climate Analytics, Germany
3 Humboldt Universität, Berlin, Germany
4 CICERO - Center for International Climate Research Oslo, Norway

E-mail: `peter.pfleiderer@climateanalytics.org`

Arpil 2023

Abstract. Without stringent reductions in emission of greenhouse gases in the coming years, an exceedance of the 1.5C temperature limit would become increasingly likely. This has given rise to so-called temperature overshoot scenarios, in which the global mean surface air temperature increase above pre-industrial levels exceeds a certain limit, i.e. 1.5C, before bringing temperatures back below that level. Despite their prominence in the climate mitigation literature, the implications of an overshoot for local climate impacts is still understudied. Here we present a comprehensive analysis of implications of an overshoot for regional temperature and precipitation changes as well as climate extremes indices. Based on a multi-model comparison from the Coupled Model Intercomparison Project (CMIP6) we find that temperature changes are largely reversible in many regions, but also report significant land-ocean and latitudinal differences after an overshoot. For precipitation, the emerging picture is less clear. In many regions the drying or wetting trend is continued throughout the overshoot irrespective of a change in the global mean temperature trend with resulting consequences for extreme precipitation. Taken together, our results indicate that even under a reversal of global mean temperature increase, regional climate changes may only be partially reversed in the decades after peak warming. We thus provide further evidence that overshooting of a warming level implies considerable risks on the regional level.

1. Introduction

The global mean surface air temperature increase above pre-industrial levels is about 1.3°C to date [1]. Without stringent emission reductions in the near-term, an exceedance of 1.5°C of global warming thus becomes increasingly likely [2]. As a consequence, so-called overshoot scenarios that temporarily exceed 1.5°C before bringing temperatures back down below that level by means of net negative CO2 emissions have risen to prominence in the mitigation literature[2, 3]. For time-lagged climate impacts such

as cryospheric changes or sea-level rise, temperature overshoot will lead to irreversible impacts [4, 5]. However, the question of reversibility is less established for changes in atmospheric variables such as temperature and precipitation.

In observations, the climate is warming globally with diverse physical impacts regionally [6] and most climate simulations are run for emission scenarios where this warming is continued. Although one would expect that regional changes reverse when climate is cooling in an overshoot scenario, there are different effects that would lead to non-linearities in the evolution of regional climate signals. While changes in some indicators such as global mean surface temperature (GMST) [7] or Arctic sea-ice can be reversed [8], a hysteresis is expected for parts of the carbon cycle, ocean heat content, or the inter-tropical convergence zone [8, 9, 10].

One factor leading to this hysteresis is the lagged response of the ocean to increased greenhouse gas concentrations in the atmosphere. While the atmosphere responds fast to changes in greenhouse gas concentrations, the ocean has a larger inertia, leading to a slower response and considerable lagged effects that will still change the climate for decades and centuries [11, 12, 13, 14]. This already implies that the transient state of a 1.5C climate is different from a climate state that is stabilized at 1.5C [15, 16]. The period after peak warming in an overshoot scenario is an extreme case where the instantaneous effect of CO2 reduction is superimposed by the lagged effect of CO2 increases from decades before peak warming.

Besides the overlay of a fast response to decreasing CO2 concentrations and a slow response to the warming of the decades before peak warming, local feedback mechanisms as well as changes in aerosol concentrations can contribute to differences in climate impacts between the period when the climate is still warming and the period after peak warming.

Here we present an overview of regional climate signals in two overshoot scenarios (SSP5-34-OS and SSP1-19) with a focus on regional climate signals that change their dependence on GMST throughout the overshoot. We analyze how regional climate signals evolve in the period before and after peak warming. By comparing the strength of the dependence of these changes on GMST before and after peak warming, we assess to what extent changes during the warming period of the overshoot are reversed during the cooling period after peak warming. This analysis gives a first overview of the physical climate impacts of overshooting a global warming goal and helps to identify hot-spot regions where considerable additional climate impacts have to be expected.

Note that, due to limited data availability, we only analyze the projections until 2100. We therefore cannot test the long-term reversibility of regional climate signals. When using the term "reversible", we mean that changes that occurred in the decades before peak warming are reversed in the decades after peak warming (30-50 years). Also, we highlight that the scenario design available to us does not allow us to establish a causal link between the overshoot and the differences in signals before and after the overshoot. Our assessment of (ir)reversibility is thereby descriptive in nature, and we investigate a range of factors that could affect different trajectories of regional climate

change before and after overshoot.

2. Data & Methods

2.1. Climate projections of overshoot scenarios

We analyze Earth System Model (ESM) simulations from the sixth phase of the Coupled Model Intercomparison Project (CMIP6 [17]) for the emission scenarios SSP5-34-OS and SSP1-19 from the Scenario Model Intercomparison Project (ScenarioMIP [18]). The SSP5-34-OS scenario is an idealized and rather unrealistic scenario where greenhouse gases are emitted at a high rate until 2040 with strong mitigation thereafter until net-zero CO_2 emissions are reached in 2065 and CO_2 concentrations in the atmosphere are further reduced from there on (see fig. 1a). The SSP1-19 is a strong mitigation scenario with only a moderate overshoot. In addition to these two overshoot scenarios, we use pre-industrial control simulations (piControl) to compare regional trends in the overshoot scenarios to trends originating from internal climate variability.

We aggregate the gridded climate projections into 46 land regions and 12 oceanic regions (see fig. 9) following the regional aggregation of the sixth assessment report of the Intergovernmental Panel on Climate Change [6]. For land regions, we only consider grid-cells that are considered as land-cells in the ESM and vice versa for ocean regions. When averaging over grid-cells of one region, grid-cells are weighted by their area within the region.
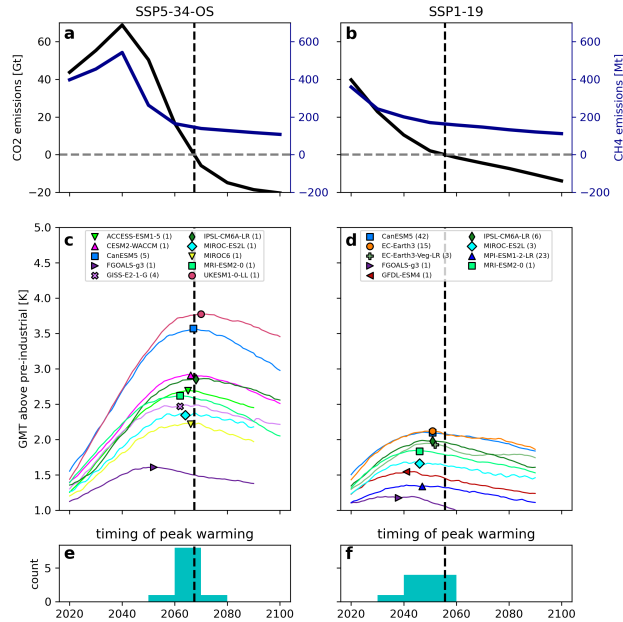

Figure 1. a: CO_2 emissions (left y-axis) and methane emissions (right y-axis) since 2020 in the SSP5-34-OS scenario. c: Global mean surface temperature (GMST) projections from CMIP6 for the SSP5-34-OS scenario. e: timing of peak warming in the CMIP6 projections of the SSP5-34-OS scenario. b: as (a) but for the SSP1-19 scenario. d: as (c) but for the SSP1-19 scenario. f: as (e) but for the SSP1-19 scenario.

Table 1. Number of simulation runs used for the main analysis based on annual temperatures and precipitation grouped by CMIP6 model and scenario. The number of available runs for other varaibles is listed in table 3.

	SSP1-19	SSP5-34-OS
ACCESS-ESM1-5		1
CESM2-WACCM		2
CanESM5	48	5
EC-Earth3	22	
EC-Earth3-Veg-LR	3	
FGOALS-g3	1	1
GFDL-ESM4	1	
GISS-E2-1-G		6
IPSL-CM6A-LR	6	1
MIROC-ES2L	3	1
MIROC6	1	1
MPI-ESM1-2-LR	30	
MRI-ESM2-0	1	1
UKESM1-0-LL		1

For our analysis, we only consider runs that have at least 20 years of data after peak warming and cool down to 0.1K below peak warming until 2100 (for 31-year averaged GMST). The ESMs as well as the number of runs for each of the scenarios are listed in table 1.

Besides monthly surface air temperature (tas) and precipitation (pr), three climate extreme indices are analyzed: the yearly maximum of daily maximum temperatures (TXx), the yearly minimum of daily minimum temperatures (TNn), and the yearly maximum daily precipitation (RX1day). These indices were calculated for runs for which daily maximum air temperature, daily minimum air temperature, and daily precipitation are available (see table 3).

Furthermore, we analyze sea surface tempratures (tos), sea ice area percentage (siconc), snow area percentage (snc), and ambient aerosol optical thickness at 550nm (od550aer) to examine potential mechanisms behind non-linearities in precipitation and temperature-based signals. Note that these variables are not available for all runs for which monthly surface air temperature and precipitation are available (see table 1). Table 3 lists the number of available runs for each variable, scenario, and ESM.

2.2. Peak warming

GMST trajectories are smoothed with a 31-year running average. In each simulation, the year with the highest smoothed GMST is identified as peak warming.

As shown in figure 1, global mean surface temperatures peak around the time when

net-zero CO_2 emissions are reached but considerable differences in the GMST response exist between different ESMs. In the SSP5-34-OS scenario, most ESMs reach peak warming between 2060 and 2070. In the SSP1-19 scenario, most ESMs reach their peak GMST between 2040 and 2060.

2.3. Period before and after peak warming

In the following, changes in regional climate signals before and after peak warming are analyzed. To allow comparability, the periods before and after peak warming have the same length (30-50 years) depending on the timing of peak warming). This period length is limited by the number of years between peak warming and the end of the simulations. For each simulation run, this period length is assessed individually. We do not consider simulations after 2100, as they are only available for a very small set of ESMs. The analyzed periods are listed for each simulation run in table 4.

2.4. Dependence of regional climate variables on GMST

For each ESM, we compare the strength of the dependence of regional climate signals on GMST before and after peak warming. We construct a simple model consisting of two linear regressions, one for the period before peak warming, and one for the period after peak warming with the condition that both regression lines have the same value in the year of peak warming. As an estimate of the dependence on GMST, use the slope β of a linear regression between the climate signal and GMST.

We test whether the trend versus GMST after peak warming β_{after} is significantly different from before (β_{before}) by comparing β_{after} to the distribution of 10,000 trends obtained by bootstrapping the data of the period before peak warming. If β_{after} is larger than the 95th or smaller than the 5th percentile of these bootstrapped trends, we consider the dependence on GMST to be significantly different after peak warming (as compared to before).

For ESMs that provide more than one run, we consider the dependence on GMST after peak warming to be significantly different as compared to the dependence on GMST before peak warming if the above-described test succeeds *and* the sign of the difference in the dependence on GMST is the same for three quarters of the runs.

Note that this statistical significance test does not exclude the possibility that the differences between before and after peak warming are a result of natural variability.
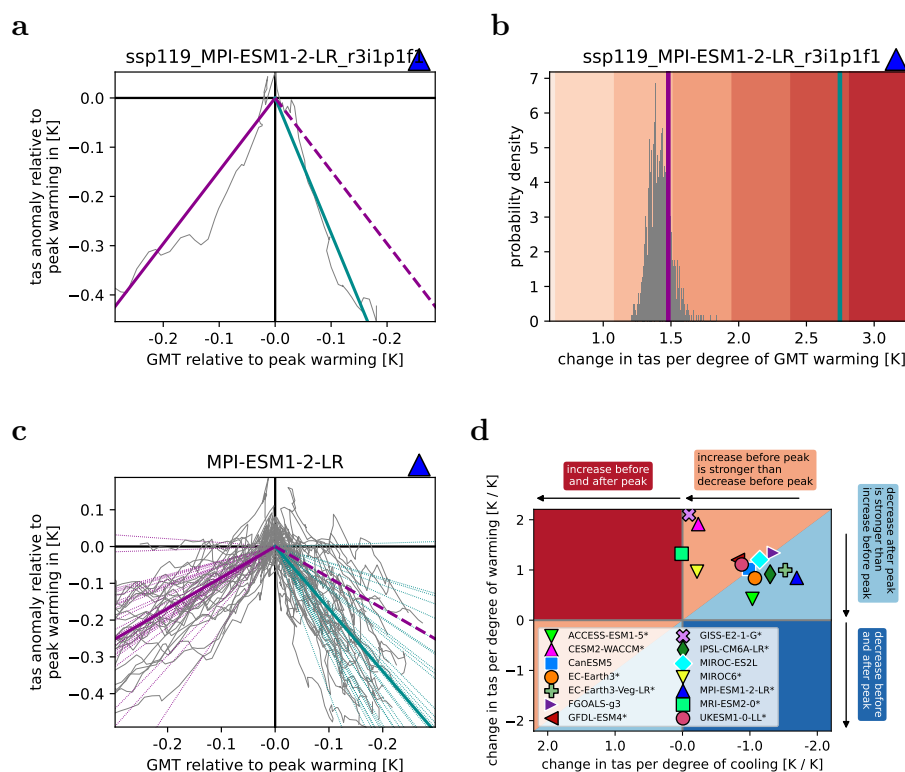
Figure 2. a: Anomalies in annual mean surface air temperature over Western Africa (gray line) projected by MPI-ESM1-2-LR (r3i1p1f1) plotted against an unconventional x-axis: GMST anomalies with respect to peak warming GMST until peak warming (vertical dashed line) and the same from there on but after peak warming. The thin purple and cyan lines indicate the trends versus GMST before and after peak warming for individual simulation runs. b: Histogram of bootstrapped trends for the period before peak warming (grey). The trends for the period before and after peak warming are indicated by cyan and purple vertical lines. c: as (a) but for all analyzed runs of MPI-ESM1-2-LR. The median of all trend lines is indicated by a thick line. For the period after peak warming, the median trend from before peak warming is shown as a thick dashed purple line. d: Overview scatter plot showing change in surface air temperature (tas) per degree of GMST warming before peak warming versus change in tas per degree of GMST cooling after peak warming. The upper left and bottom right quadrants are colored in dark red and dark blue to indicate locations where tas changes are continued after peak warming irrespective of the change in GMST trend. Markers with black outline (and asterixes in the legend) indicate that the difference between the trend before and after peak warming has been identified as statistically significant.

2.5. Detection of forced changes

The main analysis is based on forced changes in local climate signals before and after peak warming. Evaluating whether a simulated trend has been forced by changes in GMST is challenging as the changes in GMST around peak warming are relatively slow (particularly in SSP1-19) and the analyzed periods can be quite short. The simulated trends in regional climate signals can be in the range of trends that could occur as a result of internal climate variability. Therefore, for each period (before and after peak warming), we test whether the trend is common in control simulations without anthropogenic forcing (piControl). If the detected trend exceeds the 95th (or is below the 5th) percentile of all trends found over periods of identical length in piControl simulations, we reject the null-hypothesis that the detected trend is a result of internal climate variability.

The above-described method is applied to ESMs for which less than four simulations are available. If four or more simulations are available, we consider changes as forced if 75% of the simulations agree on the sign of change.

2.6. Classification of behavior around peak warming

The behavior of local climate signals around peak warming is complex and requires some tedious and in-depth analysis. Here we start by classifying the behavior around peak warming in the following flavors: "reversed", "continued", "partially reversed", "overcompensated", and "unclear".

Table 2. Classification of evolution of local climate signals around peak warming into representative types. Combining the dependence of the local climate signal on GMST before β_{before} and after β_{after} peak warming (from sec. 2.4) with the evaluation of whether the projected trends could occur as a result of natural variability (from sec. 2.5) the evolution of the climate signal is classified in the following types: reversed, continued, partially reversed, overcompensated and unclear.

Trend before and after peak outside of natural variability	$\beta_{after} \neq \beta_{before}$	$sign(\beta_{after}) = sign(\beta_{before})$	$\|\beta_{before}\| > \|\beta_{after}\|$	$\|\beta_{before}\| < \|\beta_{after}\|$	$\beta_{before} > 0$	$\beta_{before} < 0$	schematic evolution of regional climate signals over time	color coding for temperature	color coding for precipitation	
✓	x	✓	NA	NA	✓	x				reversed
✓	x	✓	NA	NA	x	✓				reversed
✓	✓	✓	✓	x	✓	x				partially reversed
✓	✓	✓	✓	x	x	✓				partially reversed
✓	✓	✓	x	✓	✓	x				overcompensated
✓	✓	✓	x	✓	x	✓				overcompensated
✓	✓	x	NA	NA	✓	x				continued
✓	✓	x	NA	NA	x	✓				continued
x	NA	NA	NA	NA	NA	NA				unclear

If no (statistically) significant change in the dependence on GMST is detected around peak warming (see section 2.4), the regional climate signal linearly follows GMST and we classify this behavior as *reversed*.

If the dependence on GMST is, however, significantly different after peak warming as compared to before, we classify the following behaviors:

- *continued*: The dependence on GMST changes in sign and the regional climate signal increases (or decreases) irrespective of the change in GMST trend.

- *partially reversed*: The dependence on GMST is significantly **lower** after peak warming and changes projected for the period where GMST is increasing are only partially reversed in the period where GMST is decreasing.

- *overcompensated*: The dependence on GMST is significantly **stronger** after peak warming and changes projected for the period before peak warming are overcompensated afterwards.

In some cases, the projected changes in the regional climate signal are not distinguishable from internal climate variability. If that is the case before as well as after peak warming, we do not classify the behavior as explained above and acknowledge that more simulations would be required by classifying the behavior as *unclear*.

Table 2 lists all the possible behaviors for temperature indicators. The color coding on the right side indicates which behaviors would lead to higher or lower temperatures at the same GMST level before and after peak warming. This color coding is used in the following to specify the behavior in an ESM. Note that these behaviors only describe the period until 2100. Changes that are not reversed until 2100 might very well be reversed later on.

3. Results

Climate projections after peak warming differ considerably from climate projections before peak warming at the same GMST level. As shown in figure 3a, the ensemble median shows regional differences in annual temperatures of up to 0.3K. Despite these strong differences, the area where ESMs agree on the sign of change is limited. For annual mean temperature, ESMs agree on warmer conditions in the eastern Southern Ocean and along the Pacific coast of South America and the El-Nino region, while for northern Africa, the Arabic peninsula and the western North Atlantic, cooler conditions are projected. A comparison between projections of different ESMs reveals that the lack of strong differences in other regions is the result of diverging behaviors in the different ESMs rather than a lack of differences between the climate after and before peak warming (see figure 3). Individual ESMs show differences of the order of 0.3K in most regions, including ESMs for which a large ensemble has been analyzed.
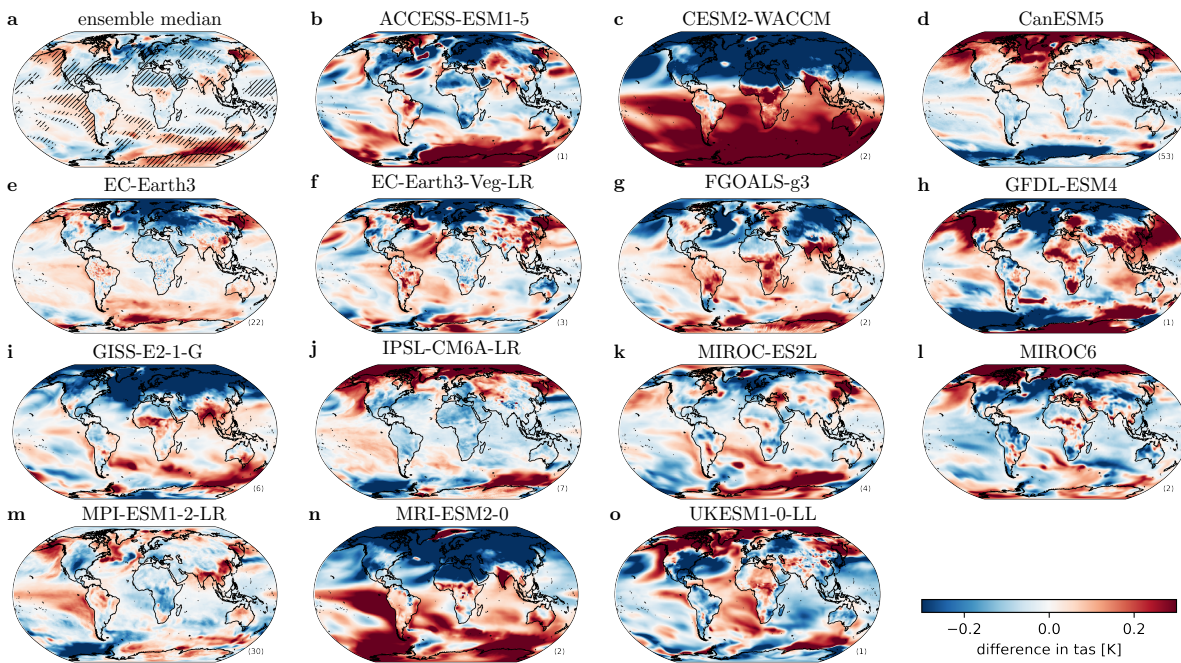

Figure 3. Difference maps comparing 30-year averaged surface air temperature (tas) after peak warming to before peak warming. Both periods have on average 0.1K cooler GMST as compared to peak warming. a: ensemble median of 14 ESMs listed in table 1 where each ESM contributes the median of it's simulation runs. Areas where at least three quarters of the ESMs agree on the sign of difference are highlighted by black hatching. b-o: as (a) but for the ensemble median of the runs of individual ESMs. The number of used runs for each ESM is indicated in the bottom right of each panel (and listed in table 1

In addition to the comparison of climate states after and before peak warming at the same GMST level, we compare how regional climate signals respond to rising GMST before and decreasing GMST after peak warming. This analysis reveals, on the one hand, that regions that are warmer after peak warming experienced a strong increase in

local temperatures during rising GMST, while in the period after peak warming these changes, are only partially reversed (see figure 4). On the other hand, regions that are cooler after peak warming experience a moderate warming in the period before peak warming that is overcompensated by a stronger cooling after peak warming.
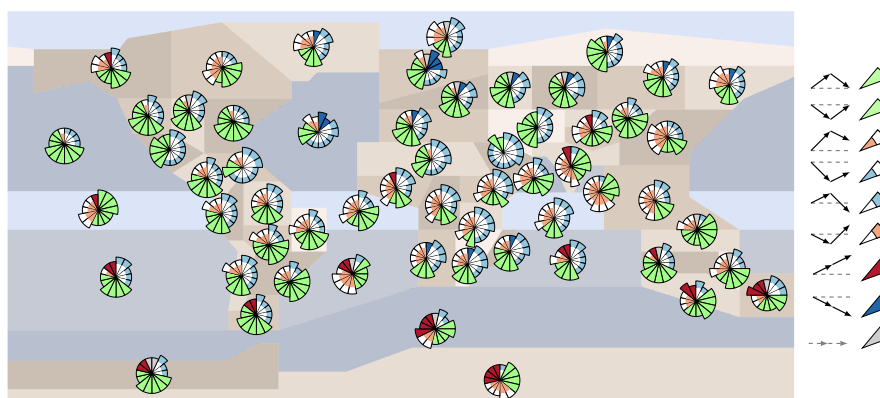

Figure 4. Evolution of regional annual mean surface air temperature around peak warming. Each regional pie-plot follows the logic of table 2. Red (blue) colors indicate that the overshoot leads to warmer (cooler) local conditions. Each ESM is represented by a circle segment. Large circle segments indicate that at least four runs could be analyzed for this ESM. Circle segments are ordered according to their colors such that ESMs with changes that cannot be differentiated from internal climate variability (gray) are grouped around 12 o clock. Following in clockwise direction come ESMs for which a continued cooling (dark blue), an overcompensated warming (light blue - white), a partially reversed cooling (white - light blue), reversed changes (green), partially reversed warming (light red - white), overcompensated cooling (white - light red) and continued warming (dark red). See figure 9 for region names. See figure 14 to see which circle segment represents which ESM.

Precipitation does not follow GMST as closely as surface air temperatures because precipitation changes are dominated by circulation changes. Therefore, the evolution of precipitation throughout the overshoot is more complex, and there are a wider variety of possible combinations of trends before and after the overshoot. In many regions, ESMs project a significant change in the dependence of precipitation on GMST, meaning that the trend in precipitation is continuing irrespective of the decrease in GMST after peak warming. In East Asia (EAS), eleven out of 14 ESMs project an increase in precipitation before peak warming that is continued after peak warming, where GMST is cooling. In Central Africa (CAF), Western Africa (WAF), and the Sahara (SAH) a strong drying is projected for the period after peak warming, overcompensating a weak increase in the period before peak warming or continuing the drying trend.

Overall, there are only a few regions where changes in the warming period of the overshoot are robustly reversed afterwards (see fig. 5). In many regions, the periods after and before peak warming are too short to identify robust changes, and more simulations would be required to analyze the evolution of precipitation changes around the overshoot. In figure 5, this is reflected by the many gray circle segments in regional
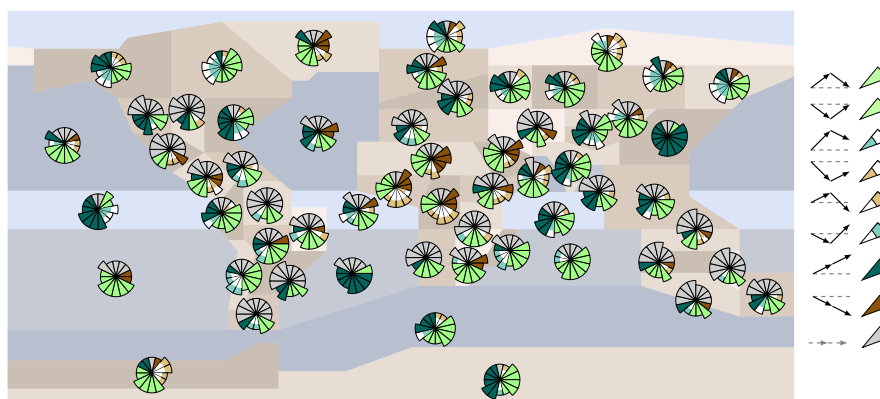
pie charts.

Figure 5. As figure 4 but for annual precipitation. Blueish colors indicate more precipitation after peak warming (brown colors less precipitation).

3.1. Climate extremes indices

As for surface air temperature, changes in temperatures of the hottest days (TXx) and the coldest nights (TNn) are projected to be reversed in many regions (see fig. 6a and 6b). For regions in the mid-latitudes of the northern hemisphere, half of the ESMs project that the increase in TXx and TNn is only partially reversed in the period after peak warming. In North America (WNA, CNA, ENA), some models even project an increase in TXx for the period where GMST is decreasing. In most tropical regions, the increase in TXx and TNn is overcompensated in the period after peak warming, leading to less intense hot extremes after the overshoot.

Intense precipitation increases around the globe as the climate warms (figure 6c). Climate model projections suggest that only in a few regions these changes are reversed after peak warming. In northern hemispheric high-latitude regions, the intensification in RX1day in the period before peak warming is only partially reversed after peak warming and in some regions the intensification trend continues while GMST is decreasing (NWN, RFE). The same behavior is found in Southeast Asia (SEA) and, to some extent, in South Asia (SAS). In most mid-latitudinal regions of the northern hemisphere, the intensification of RX1day before peak warming is overcompensated after peak warming. The opposite behavior is projected for Australia.

3.2. Potential mechanisms

One major cause for the differences in temperature and precipitation patterns between before and after peak warming are changes in sea surface temperature (SST) patterns. As shown in figure 7, surface air temperature patterns coincide with SST patterns over water and in coastal areas. Due to the considerably greater inertia of the ocean, it appears plausible that the differences in surface air temperature patterns are mainly
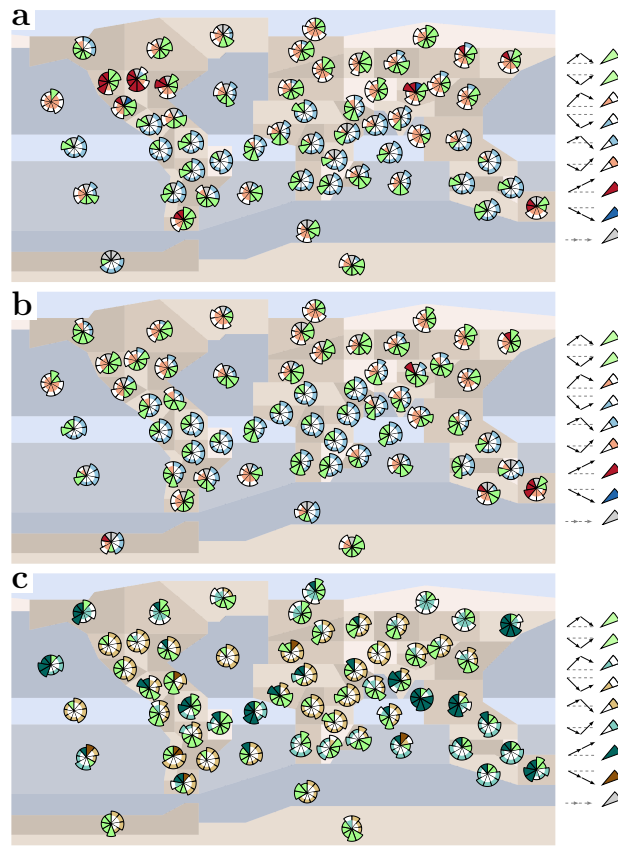
Figure 6. As figure 4 but for extreme weather indicators. a: the hottest day in a year (TXx). b: coolest night in a year (TNn). c: maximum daily precipitation in a year (RX1day).

caused by the SST patterns. Furthermore, changes in SST patterns such as the fingerprints of a weakened AMOC, more El-Nino like conditions, and a warmer Southern Ocean after peak warming modulate temperature and precipitation patterns worldwide.

Over the Southern Ocean (SOO) and the Southern Atlantic Ocean (SAO), half of the ESMs project a weaker cooling in the period after peak warming as compared to the warming before peak warming or even a continued warming. This behavior can be explained by fast and slow reactions to changes in greenhouse gas concentrations: in the fast response to increases in CO_2 concentrations, the warming over the Southern Ocean surface is suppressed, while in the slow response it is not [14, 12]. Therefore, in the period after peak warming for parts of the Southern Ocean, the fast response to the decrease in greenhouse gas emissions is dominated by the slow response to the increase in greenhouse gas emissions decades earlier.

Over the northern Atlantic, most ESMs project a stronger decrease in SSTs relative to the decrease in GMST after peak warming as compared to before peak warming. As greenhouse gas emissions rise, the Atlantic meridional overturning circulation (AMOC) weakens, leading to a cooling in the northern Atlantic and northern Europe [19, 20]. In most ESMs the AMOC recovers when global mean temperatures decrease, however,
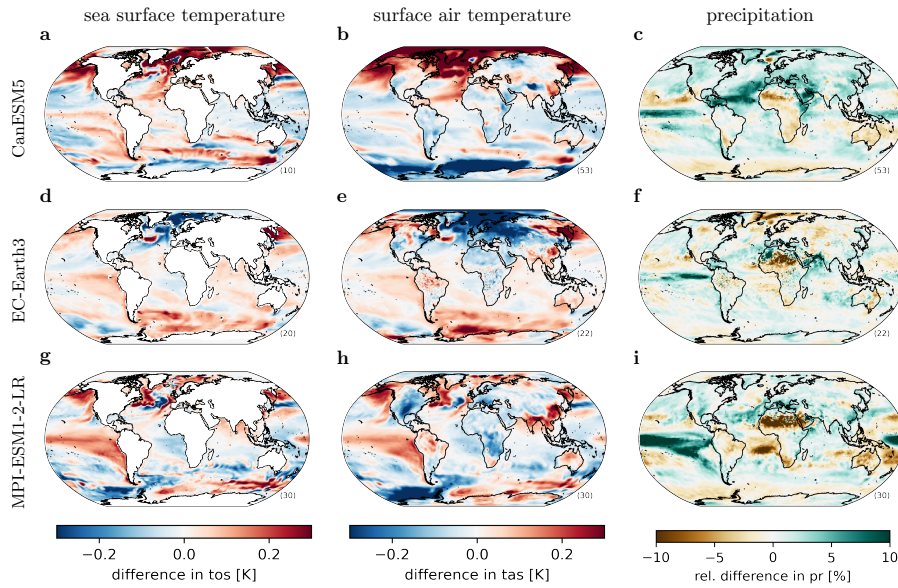
Figure 7. Difference maps comparing 30-year averages after peak warming to before peak warming. Both periods are 0.1K cooler than peak warming. First column: sea surface temperature (tos). Second column: surface air temperature (tas). Third column: precipitation (pr). All ESMs are shown in figure 19 in the Appendix.

with a considerable time lag [21]. Koven et al. (2022) show that in CESM2-WACCM the AMOC continues to decrease until 2100 in the SSP5-34-OS scenario, which explains the strong hysteresis in temperature patterns in this ESM. In CESM2-WACCM, MRI-ESM2-0, GFDL-ESM4, GISS-E2-1-G, and MIROC-ES2L, the SST difference maps show the pattern of an AMOC reduction, meaning that the AMOC is still in a weaker state in the decades after peak warming with far-reaching implications for the northern hemisphere (see figure 19).

For the Sahara (SAH), West Africa (WAF), and central Africa (CAF), drier conditions are projected for the period after peak warming as compared to before peak warming at the same GMST level. In the case of West Africa (WAF) a consistent and strong decrease in precipitation is projected by most ESMs for the period when the global climate is cooling. This drying either overcompensates the weaker wetting in the period before peak warming or continues the drying trend. This drying of western Africa is related to a southward shift of the intertropical convergence zone (ITZC). A weakening of the AMOC shifts the temperature balance between the northern and southern hemisphere leading to a southward shift of the ITZC [22]. This effect is particularly prominent in CESM2-WACCM and MRI-ESM2-0 where a strong difference in the strength of the AMOC between before and after peak warming leads to a clear hemispheric dipole pattern and a consistent shift in precipitation in the tropics (see figure 19). This finding is in line with Samset et al. [23] who show that an increase in greenhouse gas concentrations first leads to more precipitation over western Africa but to drying in the long-term and a similar effect has also been found in a longer overshoot

experiment with the community earth system model (CESM) [10].

Finally, ESMs robustly project more El-Nino like conditions for the period after peak warming as compared to before peak warming (see figure 19). For the region of the equatorial Pacific Ocean (EPO), one third of the ESMs project that the warming in the period before peak warming is only partially reversed after peak warming. CMIP6 models project a tendency towards more El-Nino like conditions as a response to increased greenhouse gas concentrations (at least for the historical period [24]). It appears as if, for a number of ESMs, this change is only partially reversed after peak warming. In those ESMs in which this El-Nino like signal is stronger in the period after peak warming as compared to before (CESM2-WACCM, EC-Earth3, GISS-E2-1-G, MRI-ESM2-0, MPI-ESM1-2-LR, see figure 19), the well-known teleconnections influence regional precipitation and temperatures around the globe [25]. Ongoing changes in El-Nino after peak warming have also been found in CMIP5 models [26] and idealized multi-century overshoot experiments with the CESM1.2 even imply a potential hysteresis behavior of ENSO under overshoot [27].

In addition to differences in regional SST patterns in the period after peak warming, aerosol concentrations are considerably lower after peak warming than before. This reduction in aerosol concentrations is most prominent in southern and eastern Asia. Over East Asia (EAS), ESMs also consistently project a continued increase in precipitation, irrespective of the reduction in GMST. The consistent increase in precipitation in the period approaching peak warming could be a result of the decrease in aerosol concentrations over eastern Asia [28, 29, 30]. Figure 8 shows that the optical thickness of aerosol at 550nm considerably decreases in East Asia (EAS), South Asia (SAS), and Southeast Asia (SEA). However, the expected warming and wetting in that region is only found in some ESMs (MPI-ESM1-2-LR, GFDL-ESM4, and GISS-E2-1-G). In most other ESMs, there does not appear to be a clear link between regions with strong reductions in aerosol concentrations (see figures 8 and 20) and the expected wetting and warming suggest that in these ESMs, aerosols are not the dominant mechanism explaining changes in regional precipitation and temperatures.

Local feedback mechanisms such as the sea ice and snow albedo effect could also lead to a lag in regional climate recovery. After peak warming, less sea ice coverage is projected for regions where SSTs are higher than before and a similar but less pronounced relationship between snow cover and surface air temperatures is projected (see figure 22). Differences in surface air temperature between after and before peak warming are generally stronger over oceans and follow closely the differences in SSTs there (see figure 19). Therefore, we assume that changes in sea ice and snow cover are mostly driven by SSTs rather than driving SSTs.

In our main analysis, we combine results from the SSP-119 and the SSP534-over scenarios. It is to expect that the response patterns also depend on the shape of the scenario as well as the absolute GMST levels reached during overshoot, which are substantially different between both scenarios. However, it appears that at least the broad spatial patterns of regional differences before and after overshoot are quite
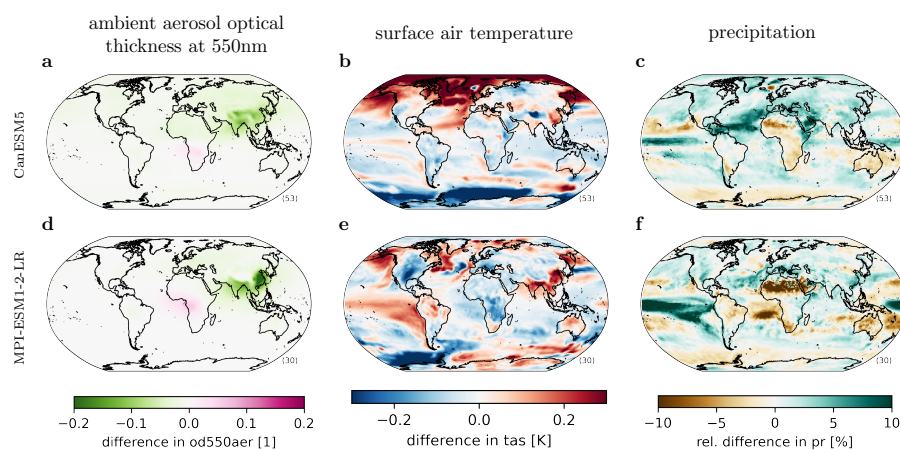
Figure 8. Difference maps comparing 30-year averaged surface air temperatures after peak warming to before peak warming. Both periods are 0.1K cooler than peak warming. First column: ambient aerosol optical thickness at 550nm. Second column: surface air temperature. Third column: precipitation. All ESMs are shown in figure 20.

consistent between both scenarios (see figure 21). This is even more remarkable as there is also a time lag in when peaking is reached of around 20 years between both scenarios (see Table 4). The most pronounced differences between the scenarios are observed in the high latitudes for CanESM5 and FGOALS-g3.

4. Discussion and conclusions

Climate projections of overshoot scenarios show that changes in regional climate signals are not reversed in the decades after peak warming, when global mean surface air temperature (GMST) decreases due to a reduction in CO2 concentration. The evolution of regional climate signals throughout the overshoot is complex and, in some regions, highly non-linear such that the dependence of regional temperature and precipitation on GMST changes considerably around peak warming.

Our analysis of the SSP1-19 and the SSP5-34-OS scenario shows that different regional temperature patterns would emerge for the period after peak warming. As a result, at the same GMST level after peak warming, some regions are projected to be considerably warmer or cooler when compared to a period with similar GMST levels before peak warming.

The evolution of regional climate signals throughout the overshoot results from the combination of different dynamic effects that potentially interact in complex ways. The overlay of the instantaneous response to the reduction in greenhouse gas concentrations after peak warming with the long-term and slow responses to emissions in the decades before peak warming [13, 12] as well as the lagged recovery of the AMOC in the period after peak warming lead to a shift in regional sea surface temperature patterns. Additionally, changes in aerosol emissions affect regional climate signals. These changes have far-reaching implications for atmospheric circulation, moisture transport, and thereby regional climate signals [31, 32, 33].

On top of these changes, local feedback mechanisms and changes in ecosystems during the overshoot might have long-term effects on local and regional climatic conditions. The representation of local effects such as changes in vegetation [34] or permafrost [35] are still a challenge for Earth System models. We therefore expect that ESMs underestimate the impacts of an overshoot on regional climate.

Here we analyze to which extent changes in the period before peak warming are reversed in the decades (40-50 years) after peak warming. Many of the effects discussed in this study may be related to lagged effects in the climate system. Whether or not these changes are projected to be reversed in the long term is beyond the scope of this study and would require more simulations going beyond 2100. Nevertheless, the time period over which these lagged effects influence regional climate signals is long enough to cause considerable climate impacts that could be avoided without an overshoot.

Earth system model projections imply considerable differences in regional climate patterns between before and after peak warming. However, the model spread is substantial and projections differ even in the sign of change before and after overshoot for many regions. The hysteresis in GMST itself, which considerably differs between the ESMs (compare figure 1), adds further to the uncertainties in projections of overshoot scenarios. Furthermore, simulations for both overshoot scenarios are only available for half of the ESMs which makes a systematic quantification of the influence of the intensity of the overshoot challenging. This highlights the need for additional and

dedicated research efforts to improve our understanding and evaluate the additional climate risks arising from an overshoot of the 1.5°C global mean temperature goal. This research should include detailed studies of the evolution of climate signals in individual ESMs. Due to the heterogeneity in ESM reactions to an overshoot scenario, a more comprehensive set of simulations of different overshoot scenarios would be required to better understand what climate impacts would arise from an overshoot [36].

Climate model projections suggest that an overshoot would cause considerable climate impacts on the regional level for several decades or potentially even longer time frames. In many regions, changes in precipitation and extreme precipitation events that are driven by the increase in global mean temperatures are expected to be continued in the period after peak warming, when global mean temperatures are already decreasing. In combination with global or regional tipping points [37, 38] and the uncertainties related to the effectiveness of methods to reduce CO2 concentrations in the atmosphere, our analysis provides further evidence that additional risks may be inferred by overshoots.

5. References

[1] K. Haustein, M. R. Allen, P. M. Forster, F. E. L. Otto, D. M. Mitchell, H. D. Matthews, and D. J. Frame. A real-time Global Warming Index. *Scientific Reports*, 7(1):15417, 2017.

[2] IPCC. Summary for policymakers. In P.R. Shukla, J. Skea, R. Slade, A. Al Khourdajie, R. van Diemen, D. McCollum, M. Pathak, S. Some, P. Vyas, R. Fradera, M. Belkacemi, A. Hasija, G. Lisboa, S. Luz, and J. Malley, editors, *Climate Change 2022: Mitigation of Climate Change. Contribution of Working Group III to the Sixth Assessment Report of the Intergovernmental Panel on Climate Change.* Cambridge University Press, Cambridge, UK and New York, NY, USA, 2022.

[3] Carl-Friedrich Schleussner, Joeri Rogelj, Michiel Schaeffer, Tabea Lissner, Rachel Licker, Erich M. Fischer, Reto Knutti, Anders Levermann, Katja Frieler, and William Hare. Science and policy characteristics of the Paris Agreement temperature goal. *Nature Climate Change*, 6(9):827–835, September 2016.

[4] Matthias Mengel, Alexander Nauels, Joeri Rogelj, and Carl-Friedrich Schleussner. Committed sea-level rise under the Paris Agreement and the legacy of delayed mitigation action. *Nature Communications*, 9(1):601, February 2018.

[5] H. Lee, K. Calvin, D. Dasgupta, G. Krinner, A. Mukherji, P. Thorne, C. Trisos, J. Romero, P. Aldunce, K. Barrett, G. Blanco, W. W. L. Cheung, S. L. Connors, F. Denton, A. Diongue-Niang, D. Dodman, M. Garschagen, O. Geden, B. Hayward, C. Jones, F. Jotzo, T. Krug, R. Lasco, J.-Y. Lee, V. Masson-Delmotte, M. Meinshausen, K. Mintenbeck, A. Mokssit, F. E. L. Otto, M. Pathak, A. Pirani, E. Poloczanska, H.-O. Pörtner, A. Revi, D. C. Roberts, J. Roy, A. C. Ruane, J. Skea, P. R. Shukla, R. Slade, A. Slangen, Y. Sokona, A. A. Sörensson, M. Tignor, D. van Vuuren, Y.-M. Wei, H. Winkler, P. Zhai, and Z. Zommers. Synthesis report of the IPCC sixth assessment report (AR6): Summary for policymakers. 2023.

[6] R. Ranasinghe, A.C. Ruane, R. Vautard, N. Arnell, E. Coppola, F.A. Cruz, S. Dessai, A.S. Islam, M. Rahimi, D. Ruiz Carrascal, J. Sillmann, M.B. Sylla, C. Tebaldi, W. Wang, and R. Zaaboul. Climate change information for regional impact and for risk assessment. In V. Masson-Delmotte, P. Zhai, A. Pirani, S.L. Connors, C. Péan, S. Berger, N. Caud, Y. Chen, L. Goldfarb, M.I. Gomis, M. Huang, K. Leitzell, E. Lonnoy, J.B.R. Matthews, T.K. Maycock, T. Waterfield, O. Yelekçi, R. Yu, and B. Zhou, editors, *Climate Change 2021: The Physical Science Basis. Contribution of Working Group I to the Sixth Assessment Report of the Intergovernmental Panel on Climate Change*, pages 1767–1926. Cambridge University Press, Cambridge, United Kingdom and New York, NY, USA, 2021.

[7] Katarzyna B. Tokarska, Kirsten Zickfeld, and Joeri Rogelj. Path Independence of Carbon Budgets When Meeting a Stringent Global Mean Temperature Target After an Overshoot. *Earth's Future*, 7(12):1283–1295, 2019.

[8] O. Boucher, P. R. Halloran, E. J. Burke, M. Doutriaux-Boucher, C. D. Jones, J. Lowe, M. A. Ringer, E. Robertson, and P. Wu. Reversibility in an Earth System model in response to CO $\less$sub$\greater$2$\less$/Sub$\greater$ concentration changes. *Environmental Research Letters*, 7(2):024013, May 2012.

[9] I. Melnikova, O. Boucher, P. Cadule, P. Ciais, T. Gasser, Y. Quilcaille, H. Shiogama, K. Tachiiri, T. Yokohata, and K. Tanaka. Carbon Cycle Response to Temperature Overshoot Beyond 2°C: An Analysis of CMIP6 Models. *Earth's Future*, 9(5):e2020EF001967, 2021.

[10] Jong-Seong Kug, Ji-Hoon Oh, Soon-Il An, Sang-Wook Yeh, Seung-Ki Min, Seok-Woo Son, Jonghun Kam, Yoo-Geun Ham, and Jongsoo Shin. Hysteresis of the intertropical convergence zone to CO2 forcing. *Nature Climate Change*, pages 1–7, December 2021.

[11] Isaac M. Held, Michael Winton, Ken Takahashi, Thomas Delworth, Fanrong Zeng, and Geoffrey K. Vallis. Probing the Fast and Slow Components of Global Warming by Returning Abruptly to Preindustrial Forcing. *Journal of Climate*, 23(9):2418–2427, May 2010.

[12] Paulo Ceppi, Giuseppe Zappa, Theodore G. Shepherd, and Jonathan M. Gregory. Fast and Slow

Components of the Extratropical Atmospheric Circulation Response to CO2 Forcing. *Journal of Climate*, 31(3):1091–1105, February 2018.

[13] Yue Dong, Kyle C. Armour, Mark D. Zelinka, Cristian Proistosescu, David S. Battisti, Chen Zhou, and Timothy Andrews. Intermodel Spread in the Pattern Effect and Its Contribution to Climate Sensitivity in CMIP5 and CMIP6 Models. *Journal of Climate*, 33(18):7755–7775, September 2020.

[14] S. Manabe, R. J. Stouffer, M. J. Spelman, and K. Bryan. Transient Responses of a Coupled Ocean–Atmosphere Model to Gradual Changes of Atmospheric CO2. Part I. Annual Mean Response. *Journal of Climate*, 4(8):785–818, August 1991.

[15] Andrew D. King, Alexander R. Borowiak, Josephine R. Brown, David J. Frame, Luke J. Harrington, Seung-Ki Min, Angeline Pendergrass, Maria Rugenstein, J. M. Kale Sniderman, and Dáithí A. Stone. Transient and Quasi-Equilibrium Climate States at 1.5°C and 2°C Global Warming. *Earth's Future*, 9(11):e2021EF002274, 2021.

[16] Sonia I. Seneviratne, Joeri Rogelj, Roland Séférian, Richard Wartenburger, Myles R. Allen, Michelle Cain, Richard J. Millar, Kristie L. Ebi, Neville Ellis, Ove Hoegh-Guldberg, Antony J. Payne, Carl-Friedrich Schleussner, Petra Tschakert, and Rachel F. Warren. The many possible climates from the Paris Agreement's aim of 1.5 °C warming. *Nature*, 558(7708):41–49, June 2018.

[17] Veronika Eyring, Sandrine Bony, Gerald A. Meehl, Catherine A. Senior, Bjorn Stevens, Ronald J. Stouffer, and Karl E. Taylor. Overview of the Coupled Model Intercomparison Project Phase 6 (CMIP6) experimental design and organization. *Geoscientific Model Development*, 9(5):1937–1958, May 2016.

[18] Brian C. O'Neill, Claudia Tebaldi, Detlef P. van Vuuren, Veronika Eyring, Pierre Friedlingstein, George Hurtt, Reto Knutti, Elmar Kriegler, Jean-Francois Lamarque, Jason Lowe, Gerald A. Meehl, Richard Moss, Keywan Riahi, and Benjamin M. Sanderson. The Scenario Model Intercomparison Project (ScenarioMIP) for CMIP6. *Geoscientific Model Development*, 9(9):3461–3482, September 2016.

[19] C. F. Schleussner, J. Runge, J. Lehmann, and A. Levermann. The role of the North Atlantic overturning and deep ocean for multi-decadal global-mean-temperature variability. *Earth System Dynamics*, 5(1):103–115, February 2014.

[20] Jonathan A. Baker, Michael J. Bell, Laura C. Jackson, Richard Renshaw, Geoffrey K. Vallis, Andrew J. Watson, and Richard A. Wood. Overturning Pathways Control AMOC Weakening in CMIP6 Models. *Geophysical Research Letters*, 50(14):e2023GL103381, 2023.

[21] Charles D. Koven, Vivek K. Arora, Patricia Cadule, Rosie A. Fisher, Chris D. Jones, David M. Lawrence, Jared Lewis, Keith Lindsay, Sabine Mathesius, Malte Meinshausen, Michael Mills, Zebedee Nicholls, Benjamin M. Sanderson, Roland Séférian, Neil C. Swart, William R. Wieder, and Kirsten Zickfeld. Multi-century dynamics of the climate and carbon cycle under both high and net negative emissions scenarios. *Earth System Dynamics*, 13(2):885–909, May 2022.

[22] E. Moreno-Chamarro, J. Marshall, and T. L. Delworth. Linking ITCZ Migrations to the AMOC and North Atlantic/Pacific SST Decadal Variability. *Journal of Climate*, 33(3):893–905, December 2019.

[23] B. H. Samset, G. Myhre, P. M. Forster, Ø. Hodnebrog, T. Andrews, G. Faluvegi, D. Fläschner, M. Kasoar, V. Kharin, A. Kirkevåg, J.-F. Lamarque, D. Olivié, T. Richardson, D. Shindell, K. P. Shine, T. Takemura, and A. Voulgarakis. Fast and slow precipitation responses to individual climate forcers: A PDRMIP multimodel study. *Geophysical Research Letters*, 43(6):2782–2791, 2016.

[24] Adam H. Sobel, Chia-Ying Lee, Steven G. Bowen, Suzana J. Camargo, Mark A. Cane, Amy Clement, Boniface Fosu, Megan Hart, Kevin A. Reed, Richard Seager, and Michael K. Tippett. Near-term tropical cyclone risk and coupled Earth system model biases. *Proceedings of the National Academy of Sciences*, 120(33):e2209631120, August 2023.

[25] Shayne McGregor, Christophe Cassou, Yu Kosaka, and Adam S. Phillips. Projected ENSO

Teleconnection Changes in CMIP6. *Geophysical Research Letters*, 49(11):e2021GL097511, 2022.

[26] Guojian Wang, Wenju Cai, Bolan Gan, Lixin Wu, Agus Santoso, Xiaopei Lin, Zhaohui Chen, and Michael J. McPhaden. Continued increase of extreme El Niño frequency long after 1.5 °C warming stabilization. *Nature Climate Change*, 7(8):568–572, August 2017.

[27] Chao Liu, Soon-Il An, Fei-Fei Jin, Jongsoo Shin, Jong-Seong Kug, Wenjun Zhang, Malte F. Stuecker, Xinyi Yuan, Aoyun Xue, Xin Geng, and Soong-Ki Kim. Hysteresis of the El Niño–Southern Oscillation to CO2 forcing. *Science Advances*, 9(31):eadh8442, August 2023.

[28] L. Liu, D. Shawki, A. Voulgarakis, M. Kasoar, B. H. Samset, G. Myhre, P. M. Forster, Ø Hodnebrog, J. Sillmann, S. G. Aalbergsjø, O. Boucher, G. Faluvegi, T. Iversen, A. Kirkevåg, J.-F. Lamarque, D. Olivié, T. Richardson, D. Shindell, and T. Takemura. A PDRMIP Multimodel Study on the Impacts of Regional Aerosol Forcings on Global and Regional Precipitation. *Journal of Climate*, 31(11):4429–4447, June 2018.

[29] B. H. Samset, M. Sand, C. J. Smith, S. E. Bauer, P. M. Forster, J. S. Fuglestvedt, S. Osprey, and C.-F. Schleussner. Climate Impacts From a Removal of Anthropogenic Aerosol Emissions. *Geophysical Research Letters*, 45(2):1020–1029, January 2018.

[30] Jana Sillmann, Camilla W. Stjern, Gunnar Myhre, Bjørn H. Samset, Øivind Hodnebrog, Timothy Andrews, Olivier Boucher, Gregory Faluvegi, Piers Forster, Matthew R. Kasoar, Viatcheslav V. Kharin, Alf Kirkevåg, Jean-Francois Lamarque, Dirk J. L. Olivié, Thomas B. Richardson, Drew Shindell, Toshihiko Takemura, Apostolos Voulgarakis, and Francis W. Zwiers. Extreme wet and dry conditions affected differently by greenhouse gases and aerosols. *npj Climate and Atmospheric Science*, 2(1):1–7, July 2019.

[31] Jie He and Brian J. Soden. A re-examination of the projected subtropical precipitation decline. *Nature Climate Change*, 7(1):53–57, January 2017.

[32] Giuseppe Zappa, Paulo Ceppi, and Theodore G. Shepherd. Time-evolving sea-surface warming patterns modulate the climate change response of subtropical precipitation over land. *Proceedings of the National Academy of Sciences*, 117(9):4539–4545, March 2020.

[33] Hongyu Hou, Xia Qu, and Gang Huang. Reversal Asymmetry of Rainfall Change Over the Indian Ocean During the Radiative Forcing Increase and Stabilization. *Earth's Future*, 9(10), October 2021.

[34] Xiang Song, Dan-Yun Wang, Fang Li, and Xiao-Dong Zeng. Evaluating the performance of CMIP6 Earth system models in simulating global vegetation structure and distribution. *Advances in Climate Change Research*, 12(4):584–595, August 2021.

[35] Eleanor J. Burke, Yu Zhang, and Gerhard Krinner. Evaluating permafrost physics in the Coupled Model Intercomparison Project 6 (CMIP6) models and their sensitivity to climate change. *The Cryosphere*, 14(9):3155–3174, September 2020.

[36] Malte Meinshausen, Carl-Friedrich Schleussner, Kathleen Beyer, Greg Bodeker, Olivier Boucher, Josep G. Canadell, John S. Daniel, Aïda Diongue-Niang, Fatimah Driouech, Erich Fischer, Piers Forster, Michael Grose, Gerrit Hansen, Zeke Hausfather, Tatiana Ilyina, Jarmo S. Kikstra, Joyce Kimutai, Andrew King, June-Yi Lee, Chris Lennard, Tabea Lissner, Alexander Nauels, Glen P. Peters, Anna Pirani, Gian-Kasper Plattner, Hans Pörtner, Joeri Rogelj, Maisa Rojas, Joyashree Roy, Bjørn H. Samset, Benjamin M. Sanderson, Roland Séférian, Sonia Seneviratne, Christopher J. Smith, Sophie Szopa, Adelle Thomas, Diana Urge-Vorsatz, Guus J. M. Velders, Tokuta Yokohata, Tilo Ziehn, and Zebedee Nicholls. A perspective on the next generation of Earth system model scenarios: Towards representative emission pathways (REPs). *Geoscientific Model Development Discussions*, pages 1–40, September 2023.

[37] Nico Wunderling, Ricarda Winkelmann, Johan Rockström, Sina Loriani, David I. Armstrong McKay, Paul D. L. Ritchie, Boris Sakschewski, and Jonathan F. Donges. Global warming overshoots increase risks of climate tipping cascades in a network model. *Nature Climate Change*, 13(1):75–82, January 2023.

[38] Uta Kloenne, Alexander Nauels, Pam Pearson, Robert M. DeConto, Helen S. Findlay, Gustaf Hugelius, Alexander Robinson, Joeri Rogelj, Edward A. G. Schuur, Julienne Stroeve, and Carl-

Friedrich Schleussner. Only halving emissions by 2030 can minimize risks of crossing cryosphere thresholds. *Nature Climate Change*, 13(1):9–11, January 2023.

[39] Peter Pfleiderer. Regional climate signals in overshoot scenarios. October 2023.

6. Conflict of interests

The authors declare no conflict of interests.

7. Data availability

The analyzed CMIP6 simulations are freely available under `https://esgf-node.llnl.gov/search/cmip6/`.

8. Code availability

The python scripts used to analyze the CMIP6 simulations and to produce all figures and results of this study can be found under `https://zenodo.org/record/8420065`[39].

9. Funding acknowledgements
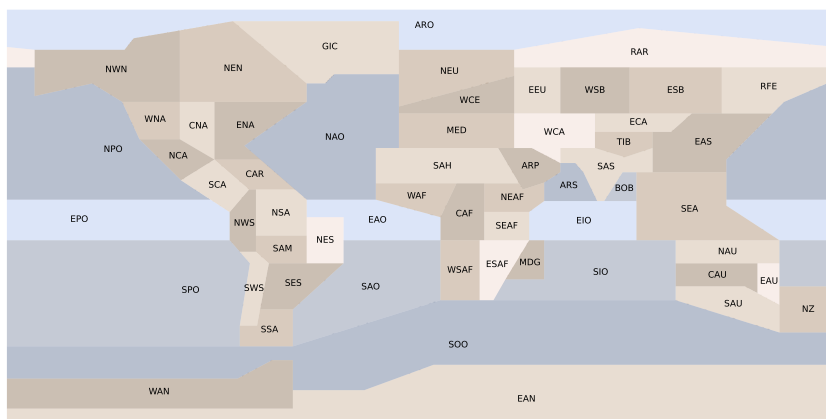
10. Appendix

Figure 9. Regions as used in the 6th assessment report of the Intergovernemental Panel on Climate Change.
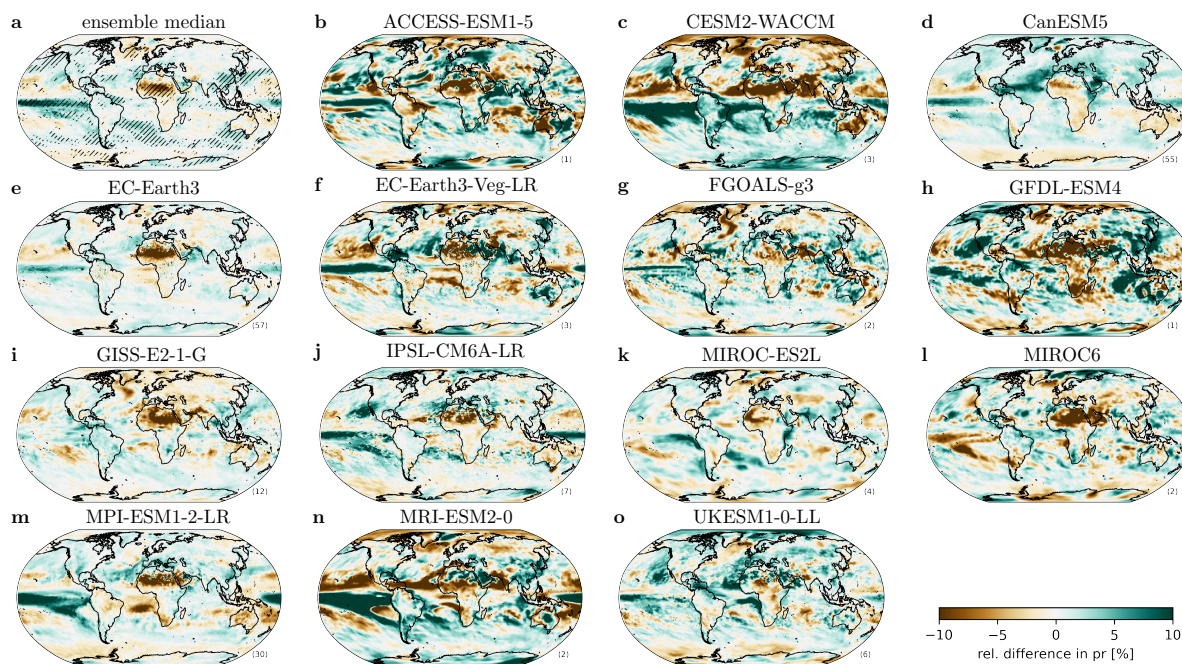

Figure 10. As figure 3 but for precipitation.

Table 3. Number of analyzed simulation runs grouped by CMIP6 model and scenario.

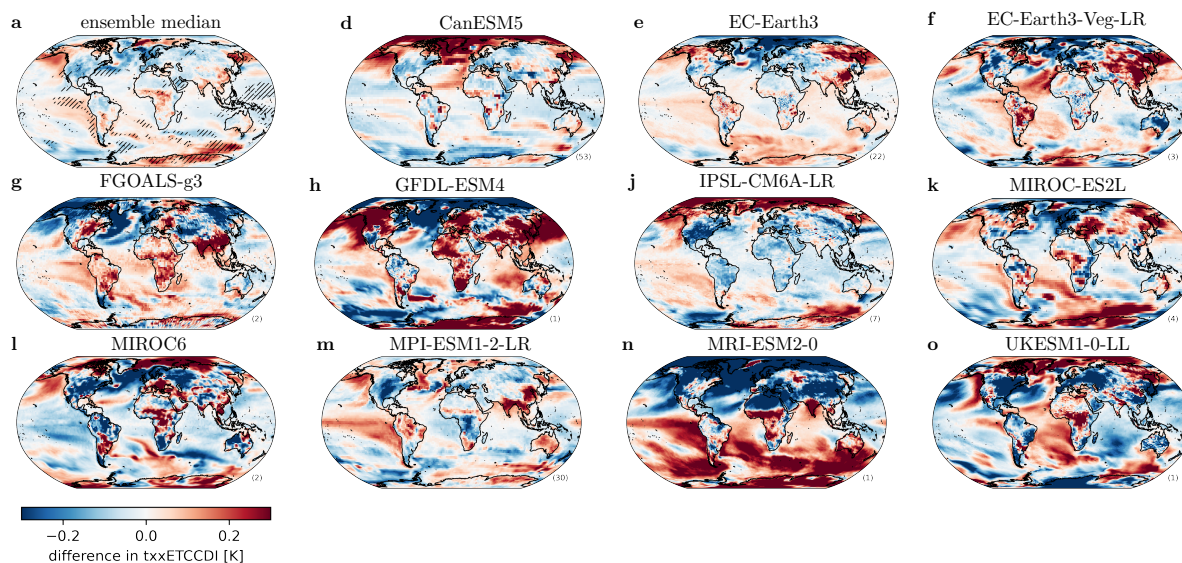|	surface air temperature (monthly)		precipitation (monthly)		yearly maximum of daily maximum temperatures (TXx)		yearly minimum of daily minimum temperatures (TNn)		yearly maximum daily precipitation (RX1day)		sea surface temperature (monthly)		ambient aerosol optical thickness at 550nm		sea-ice area percentage		snow area percentage	
	SSP1-19	SSP5-34-OS	SSP1-19	SSP5-34-OS	SSP1-19	SSP5-34-OS	SSP1-19	SSP5-34-OS	SSP1-19	SSP5-34-OS	SSP1-19	SSP5-34-OS	SSP1-19	SSP5-34-OS	SSP1-19	SSP5-34-OS	SSP1-19	SSP5-34-OS
ACCESS-ESM1-5		1		1								1				1		
CESM2-WACCM		2		2								2		2		2		
CanESM5	48	5	48	5	48		48		48	5	5	5	48	5	7	5		
EC-Earth3	22		22		22		22		22		22	0			0	0		
EC-Earth3-Veg-LR	3		3		3		3		3		3				1			
FGOALS-g3	1	1	1	1							1	1			1	1		
GFDL-ESM4	1		1		1		1		1		1		1		1			
GISS-E2-1-G		6		6							0	1		5				
IPSL-CM6A-LR	6	1	6	1	6		6		6		6	1	6	1	6	1		
MIROC-ES2L	3	1	3	1	3	1	3	1	3	1		1	3	1		1		
MIROC6	1	1	1	1	1		1		1	1	1	1			1	1		
MPI-ESM1-2-LR	30		30		30		30		30		30		30		30			
MRI-ESM2-0	1	1	1	1	1		1		1	1	1	1	1	1	1	1		
UKESM1-0-LL		1		1							0	1	0	1	0	0		

Figure 11. As figure 3 but for the hottest day in a year (TXx). Note that for TXx less runs were available than for surface air temperatures.
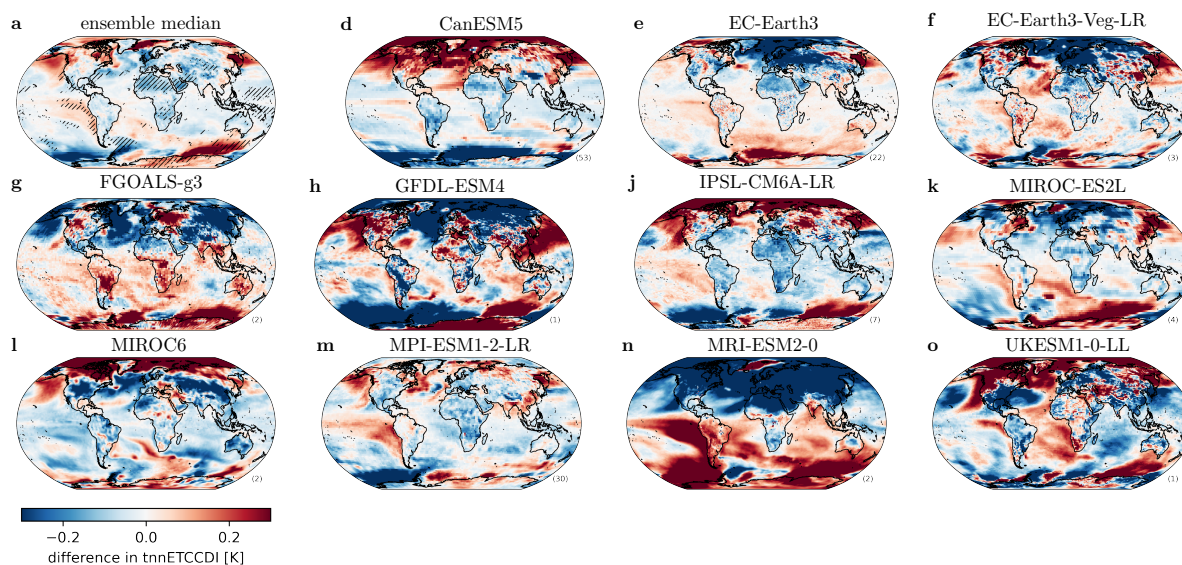
Figure 12. As figure 3 but for the coldest night in a year (TNn). Note that for TNn less runs were available than for surface air temperatures.
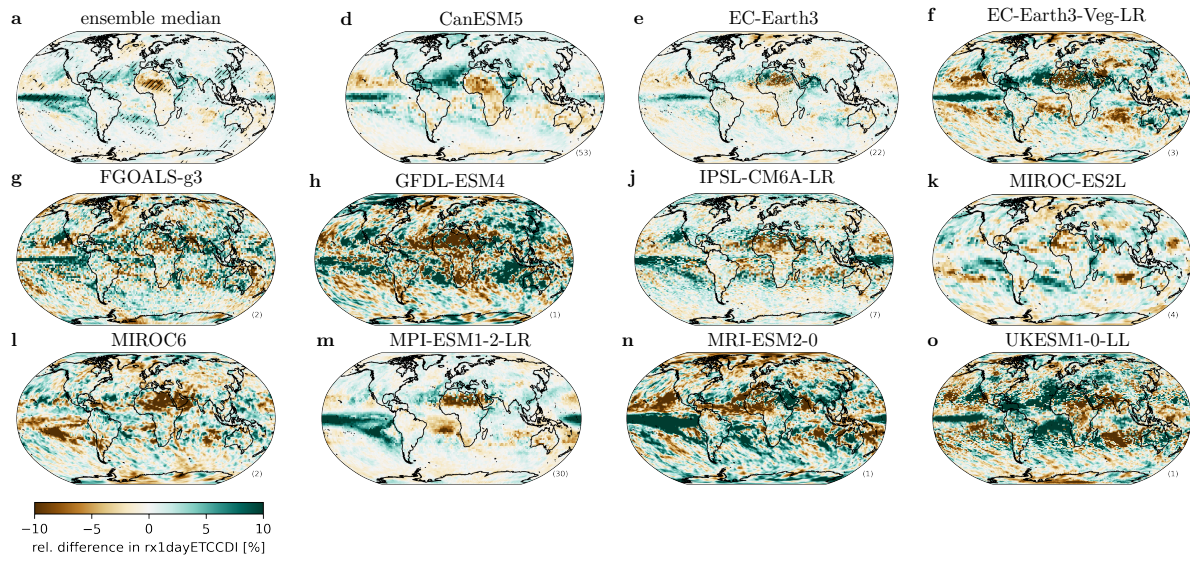
Figure 13. As figure 3 but for the yearly maximum daily precipitation (RX1day). Note that for RX1day less runs were available than for surface air temperatures.
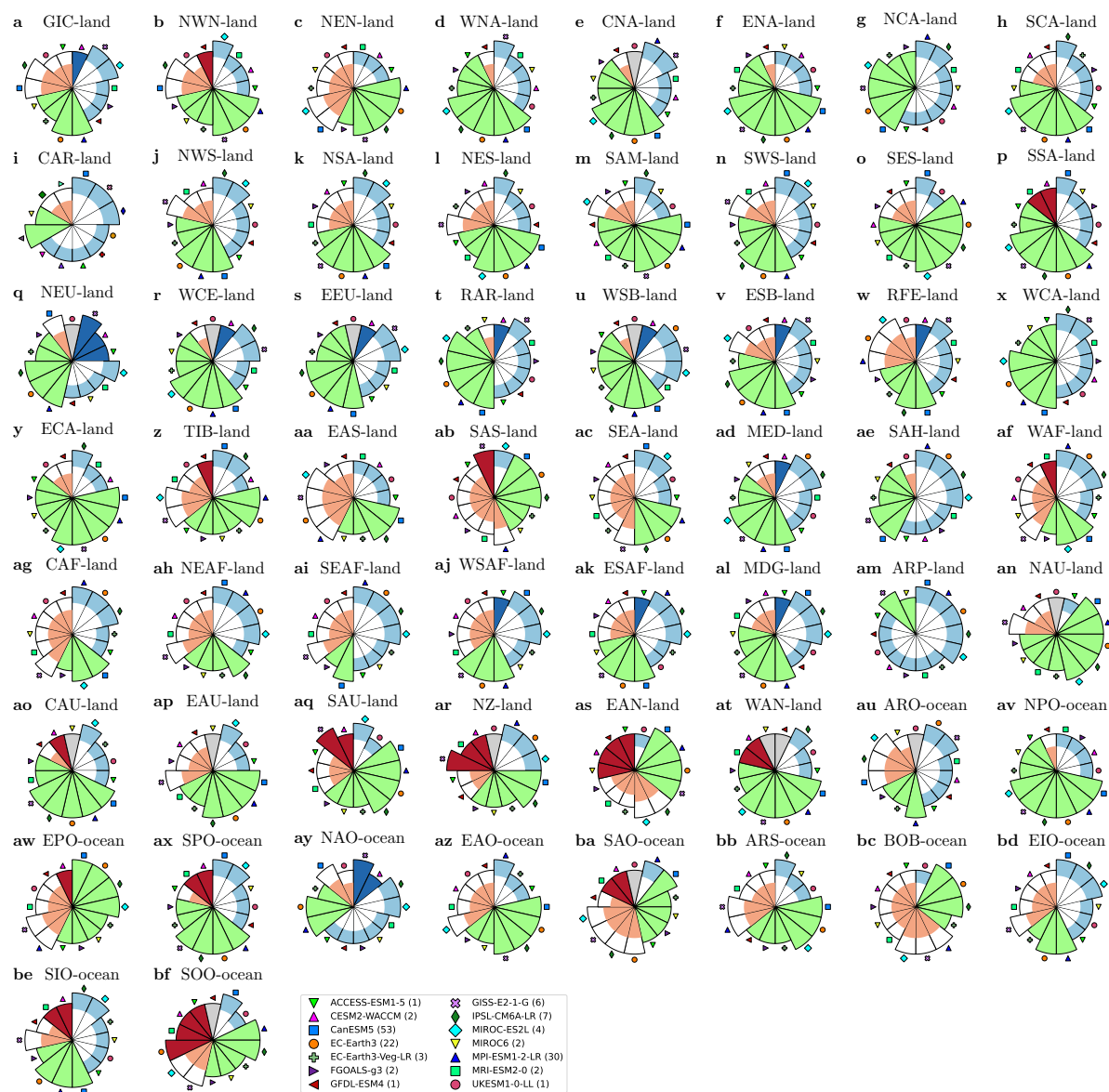
Figure 14. Evolution of surface air temperatures throughout the overshoot for all regions of figure 9. Each ESM is represented by one piece of the pie following the logic of table 2.
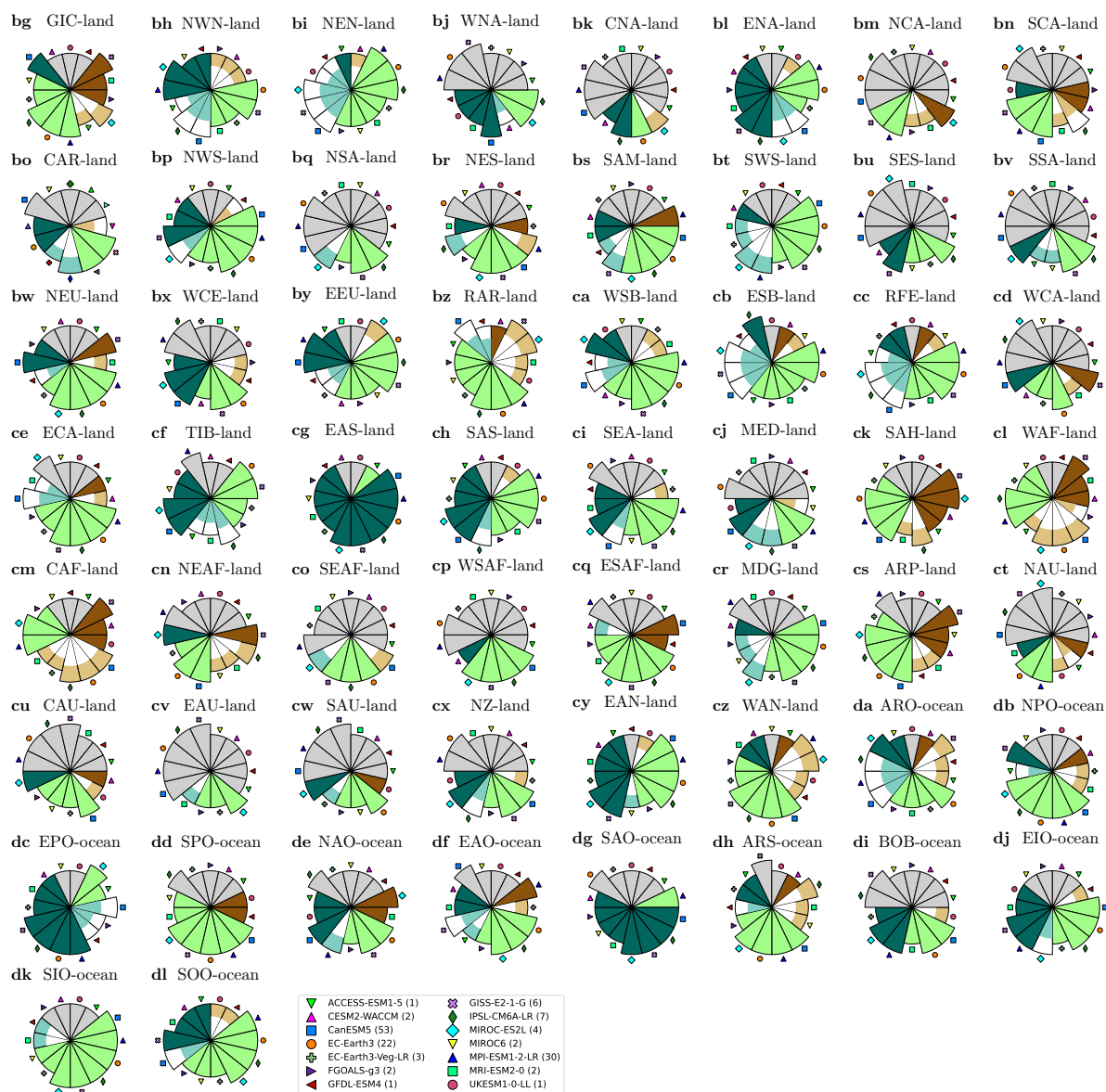
Figure 15. As figure 14 but for precipitation.
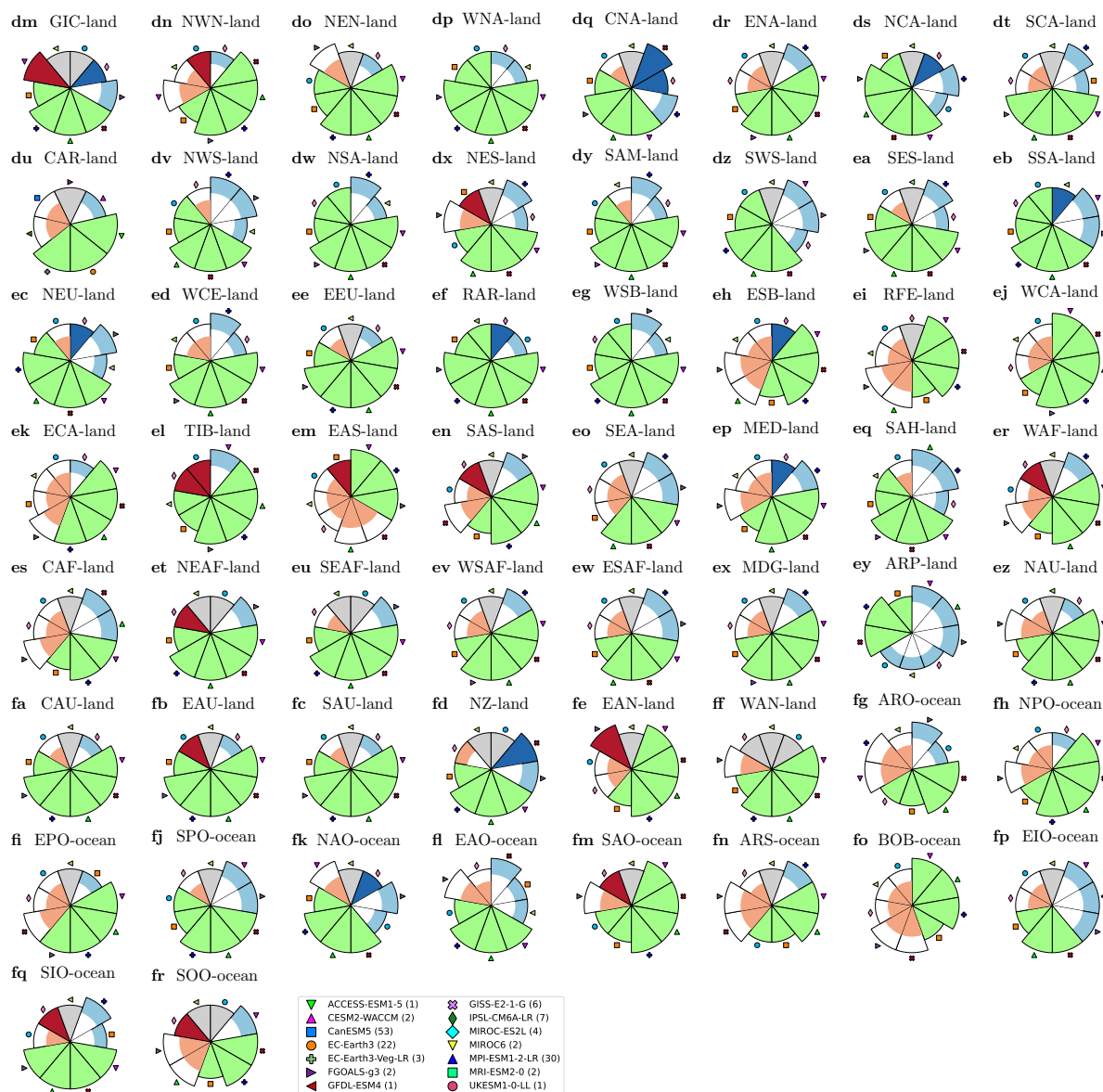
Figure 16. As figure 14 but for TXx.
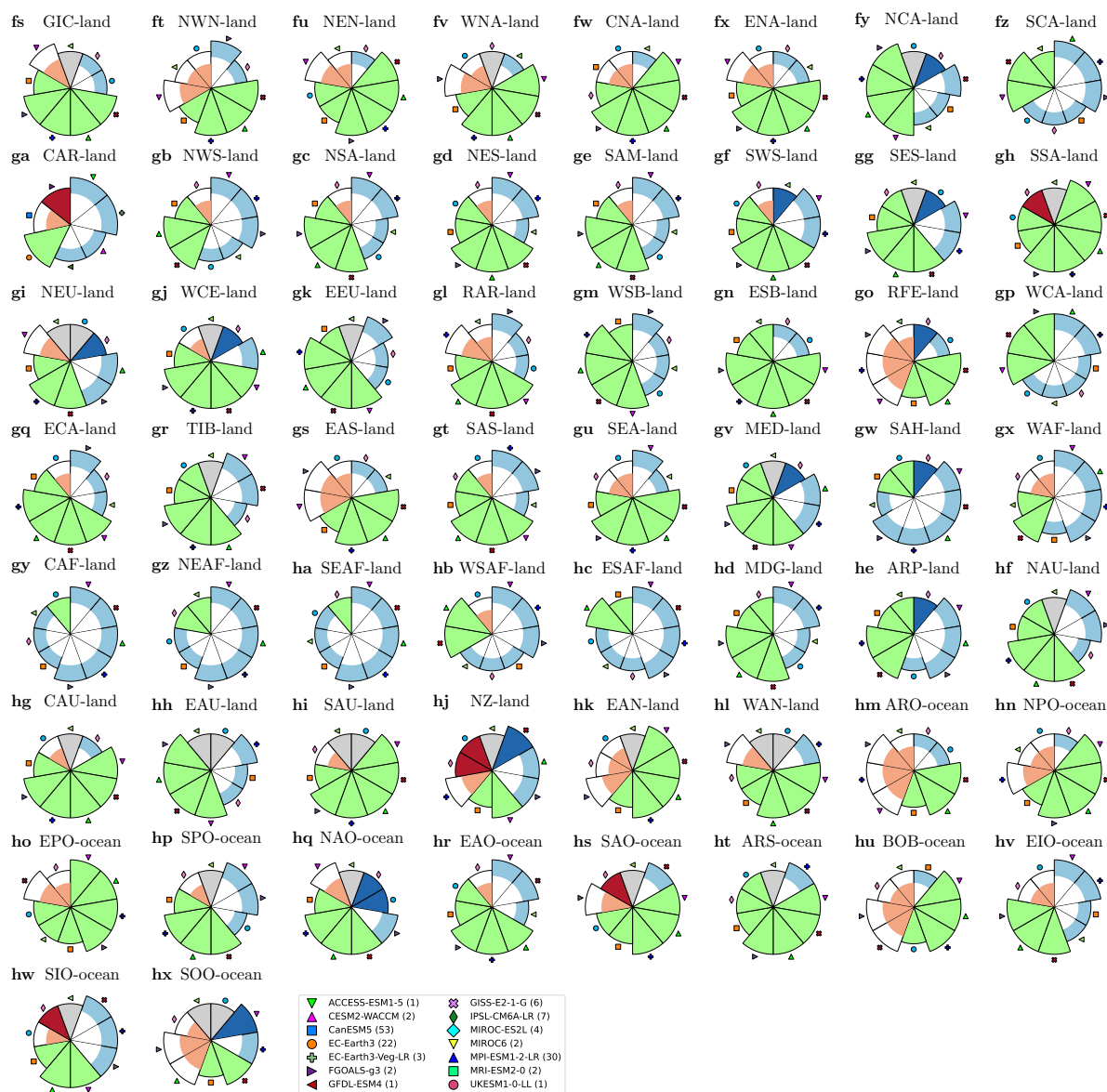
Figure 17. As figure 14 but for TNn.
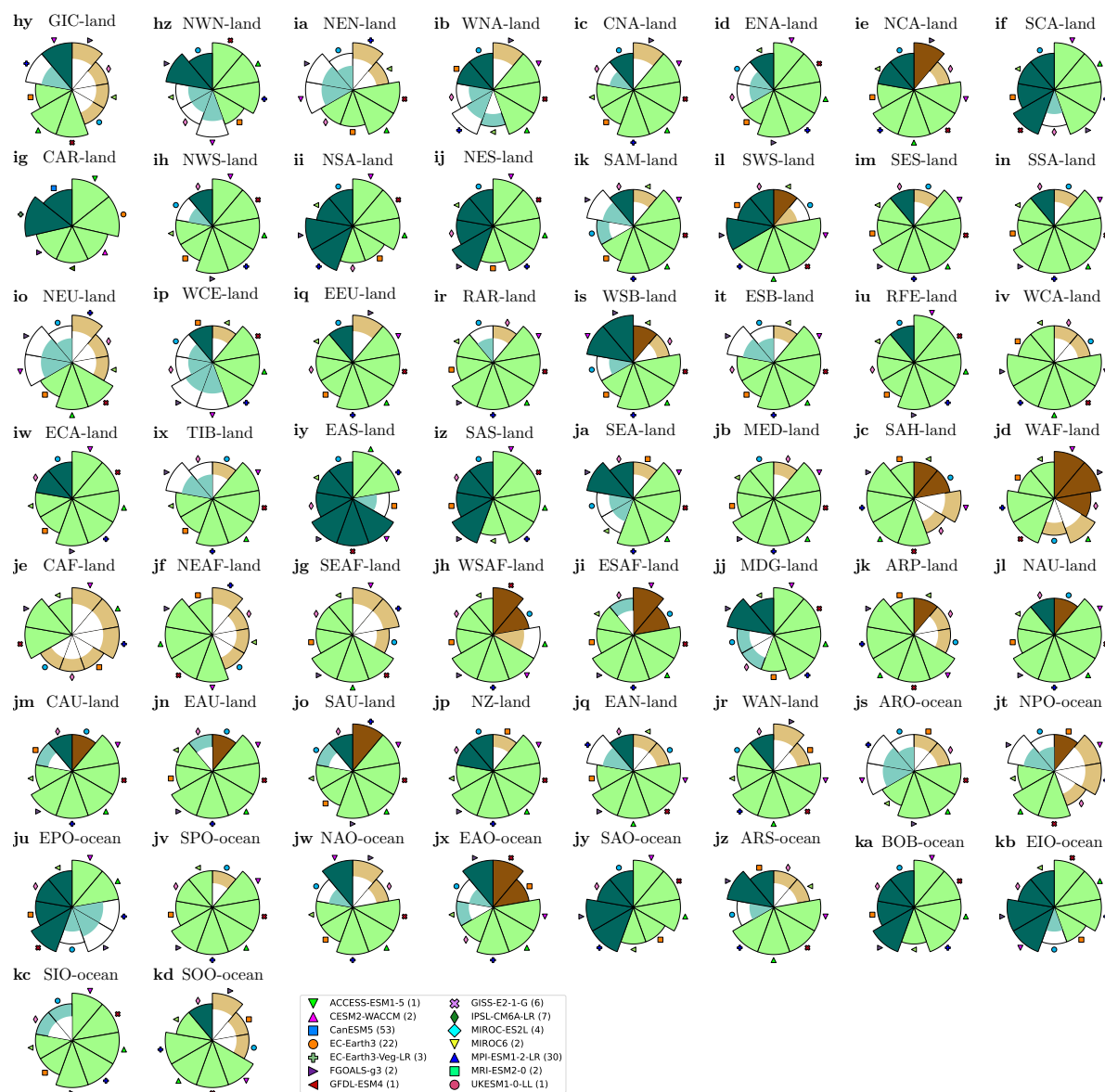
Figure 18. As figure 14 but for RX1day.
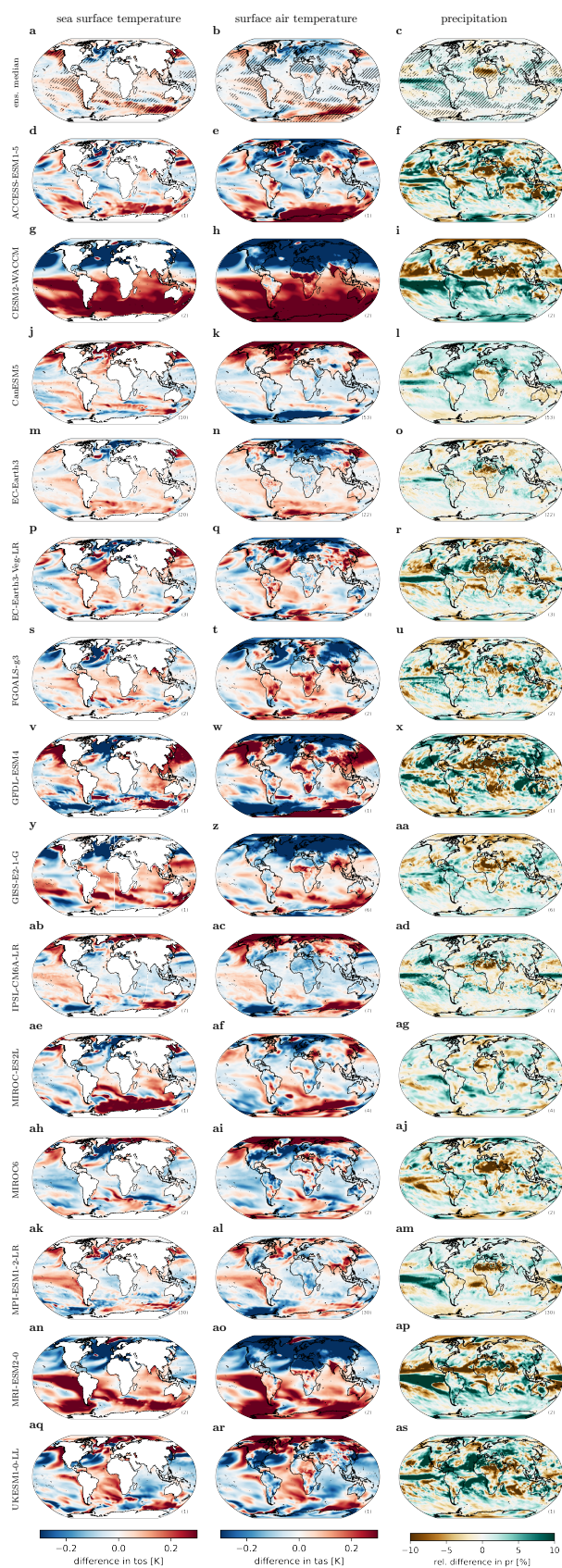
Figure 19. Difference maps comparing 30-year averages after peak warming to before peak warming. Both periods are 0.1K cooler than peak warming. First column: sea surface temperature. Second column: surface air temperature. Third column: precipitation.
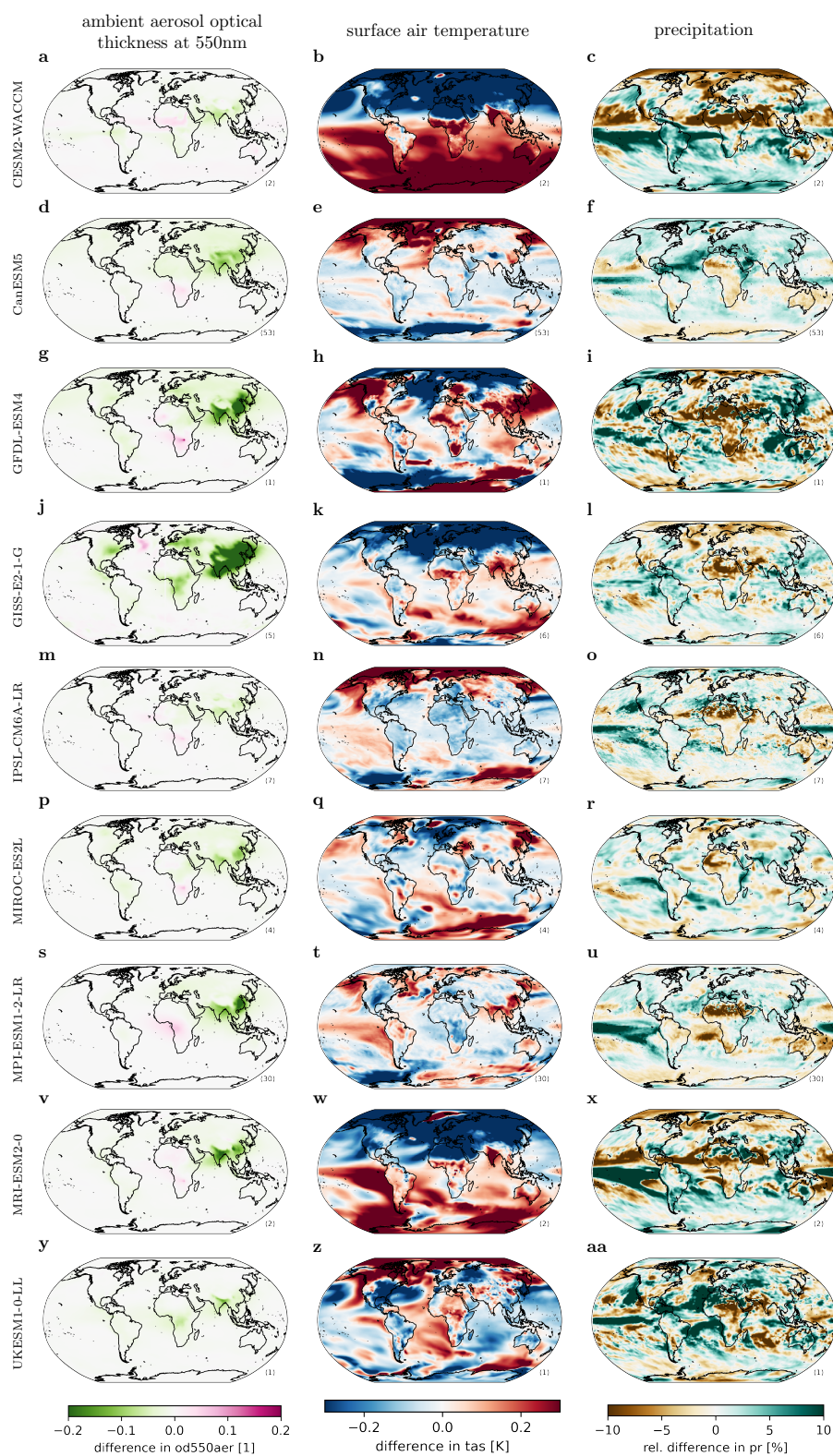
Figure 20. Difference maps comparing 30-year averages after peak warming to before peak warming. Both periods are 0.1K cooler than peak warming. First column: ambient aerosol optical thickness at 550nm. Second column: surface air temperature. Third column: precipitation.
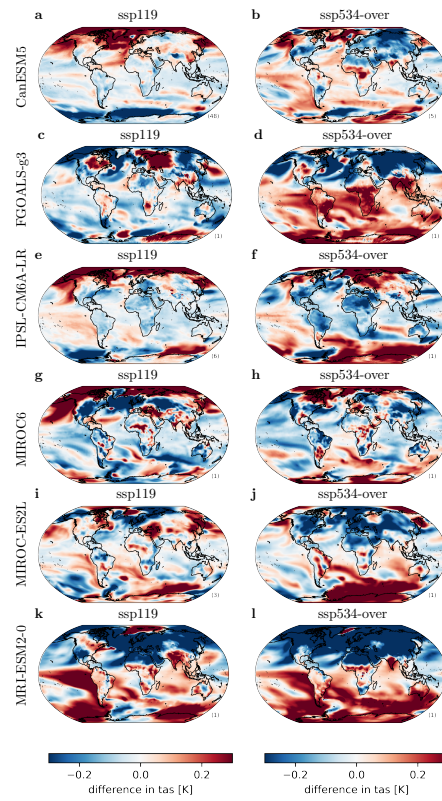
Figure 21. Difference maps comparing 30-year averaged surface air temperatures after peak warming to before peak warming. Both periods are 0.1K cooler than peak warming. Simulations for the SSP-119 scenario in on the left and SSP-534-over on the right.

Figure 22. Difference maps comparing 30-year averages after peak warming to before peak warming for the Arctic. Both periods are 0.1K cooler than peak warming. First column: sea surface temperature. Second column: sea ice coverage in area percentage. Third column: snow cover in area percentage. Fourth column: surface air temperature.

Table 4: Timing of peak warming and analyzed period before and
after peak warming for all 136 analyzed simulation runs.

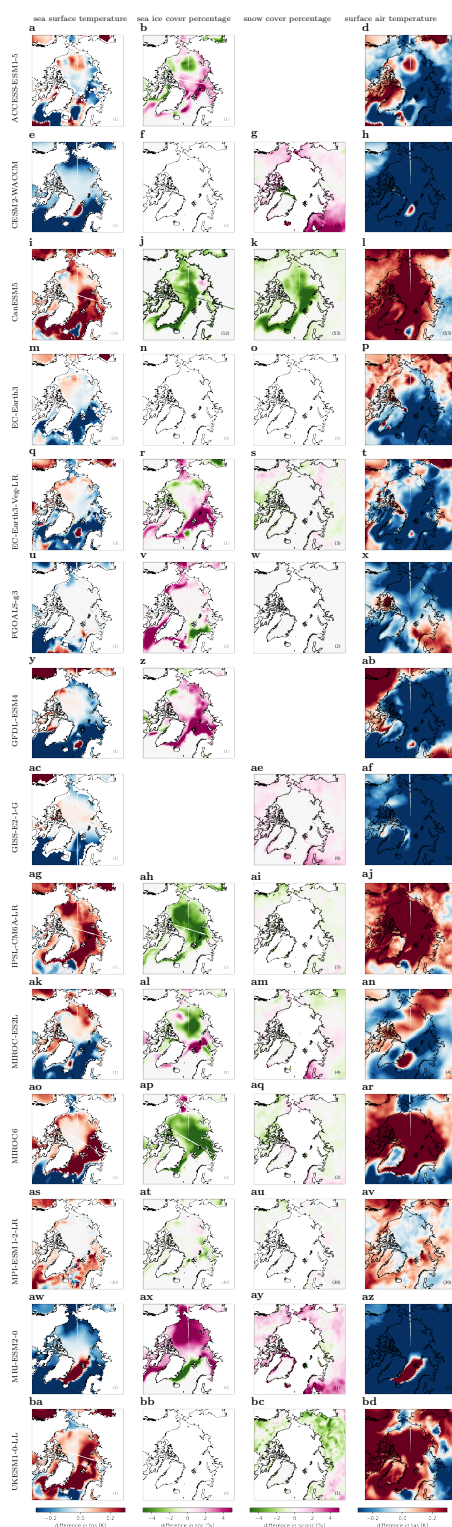| scenario	ESM	run	peak year	period before	period after	period length
ssp119	CanESM5	r10i1p1f1	2055	2010-2055	2055-2100	45
ssp119	CanESM5	r10i1p2f1	2060	2020-2060	2060-2100	40
ssp119	CanESM5	r11i1p1f1	2052	2004-2052	2052-2100	48
ssp119	CanESM5	r11i1p2f1	2052	2004-2052	2052-2100	48
ssp119	CanESM5	r12i1p1f1	2048	1996-2048	2048-2100	52
ssp119	CanESM5	r12i1p2f1	2054	2008-2054	2054-2100	46
ssp119	CanESM5	r13i1p1f1	2046	1992-2046	2046-2100	54
ssp119	CanESM5	r13i1p2f1	2049	1998-2049	2049-2100	51
ssp119	CanESM5	r14i1p1f1	2054	2008-2054	2054-2100	46
ssp119	CanESM5	r14i1p2f1	2055	2010-2055	2055-2100	45
ssp119	CanESM5	r15i1p1f1	2048	1996-2048	2048-2100	52
ssp119	CanESM5	r15i1p2f1	2057	2014-2057	2057-2100	43
ssp119	CanESM5	r16i1p1f1	2056	2012-2056	2056-2100	44
ssp119	CanESM5	r16i1p2f1	2050	2000-2050	2050-2100	50
ssp119	CanESM5	r17i1p1f1	2058	2016-2058	2058-2100	42
ssp119	CanESM5	r17i1p2f1	2052	2004-2052	2052-2100	48
ssp119	CanESM5	r18i1p1f1	2052	2004-2052	2052-2100	48
ssp119	CanESM5	r18i1p2f1	2050	2000-2050	2050-2100	50
ssp119	CanESM5	r19i1p1f1	2048	1996-2048	2048-2100	52
ssp119	CanESM5	r19i1p2f1	2048	1996-2048	2048-2100	52
ssp119	CanESM5	r1i1p1f1	2057	2014-2057	2057-2100	43
ssp119	CanESM5	r1i1p2f1	2050	2000-2050	2050-2100	50
ssp119	CanESM5	r20i1p1f1	2054	2008-2054	2054-2100	46
ssp119	CanESM5	r20i1p2f1	2052	2004-2052	2052-2100	48
ssp119	CanESM5	r21i1p1f1	2058	2016-2058	2058-2100	42
ssp119	CanESM5	r22i1p1f1	2056	2012-2056	2056-2100	44
ssp119	CanESM5	r22i1p2f1	2053	2006-2053	2053-2100	47
ssp119	CanESM5	r23i1p1f1	2054	2008-2054	2054-2100	46
ssp119	CanESM5	r23i1p2f1	2054	2008-2054	2054-2100	46
ssp119	CanESM5	r24i1p1f1	2048	1996-2048	2048-2100	52
ssp119	CanESM5	r24i1p2f1	2052	2004-2052	2052-2100	48
ssp119	CanESM5	r25i1p1f1	2055	2010-2055	2055-2100	45
ssp119	CanESM5	r2i1p1f1	2053	2006-2053	2053-2100	47
ssp119	CanESM5	r2i1p2f1	2055	2010-2055	2055-2100	45
ssp119	CanESM5	r3i1p1f1	2055	2010-2055	2055-2100	45
ssp119	CanESM5	r3i1p2f1	2053	2006-2053	2053-2100	47
ssp119	CanESM5	r4i1p1f1	2054	2008-2054	2054-2100	46
ssp119	CanESM5	r4i1p2f1	2058	2016-2058	2058-2100	42
ssp119	CanESM5	r5i1p1f1	2055	2010-2055	2055-2100	45
ssp119	CanESM5	r5i1p2f1	2051	2002-2051	2051-2100	49
ssp119	CanESM5	r6i1p1f1	2053	2006-2053	2053-2100	47
ssp119	CanESM5	r6i1p2f1	2054	2008-2054	2054-2100	46
ssp119	CanESM5	r7i1p1f1	2054	2008-2054	2054-2100	46
ssp119	CanESM5	r7i1p2f1	2056	2012-2056	2056-2100	44
ssp119	CanESM5	r8i1p1f1	2051	2002-2051	2051-2100	49
ssp119	CanESM5	r8i1p2f1	2052	2004-2052	2052-2100	48
ssp119	CanESM5	r9i1p1f1	2050	2000-2050	2050-2100	50

ssp119	CanESM5	r9i1p2f1	2059	2018-2059	2059-2100	41
ssp119	EC-Earth3-Veg-LR	r1i1p1f1	2044	1988-2044	2044-2100	56
ssp119	EC-Earth3-Veg-LR	r2i1p1f1	2051	2002-2051	2051-2100	49
ssp119	EC-Earth3-Veg-LR	r3i1p1f1	2065	2030-2065	2065-2100	35
ssp119	EC-Earth3	r102i1p1f1	2044	1988-2044	2044-2100	56
ssp119	EC-Earth3	r105i1p1f1	2048	1996-2048	2048-2100	52
ssp119	EC-Earth3	r106i1p1f1	2053	2006-2053	2053-2100	47
ssp119	EC-Earth3	r111i1p1f1	2052	2004-2052	2052-2100	48
ssp119	EC-Earth3	r112i1p1f1	2050	2000-2050	2050-2100	50
ssp119	EC-Earth3	r117i1p1f1	2050	2000-2050	2050-2100	50
ssp119	EC-Earth3	r118i1p1f1	2056	2012-2056	2056-2100	44
ssp119	EC-Earth3	r119i1p1f1	2041	1982-2041	2041-2100	59
ssp119	EC-Earth3	r124i1p1f1	2053	2006-2053	2053-2100	47
ssp119	EC-Earth3	r130i1p1f1	2052	2004-2052	2052-2100	48
ssp119	EC-Earth3	r132i1p1f1	2045	1990-2045	2045-2100	55
ssp119	EC-Earth3	r133i1p1f1	2062	2024-2062	2062-2100	38
ssp119	EC-Earth3	r135i1p1f1	2050	2000-2050	2050-2100	50
ssp119	EC-Earth3	r136i1p1f1	2058	2016-2058	2058-2100	42
ssp119	EC-Earth3	r141i1p1f1	2054	2008-2054	2054-2100	46
ssp119	EC-Earth3	r142i1p1f1	2052	2004-2052	2052-2100	48
ssp119	EC-Earth3	r143i1p1f1	2050	2000-2050	2050-2100	50
ssp119	EC-Earth3	r144i1p1f1	2052	2004-2052	2052-2100	48
ssp119	EC-Earth3	r146i1p1f1	2053	2006-2053	2053-2100	47
ssp119	EC-Earth3	r147i1p1f1	2055	2010-2055	2055-2100	45
ssp119	EC-Earth3	r148i1p1f1	2056	2012-2056	2056-2100	44
ssp119	EC-Earth3	r150i1p1f1	2050	2000-2050	2050-2100	50
ssp119	FGOALS-g3	r1i1p1f1	2036	1972-2036	2036-2100	64
ssp119	GFDL-ESM4	r1i1p1f1	2043	1986-2043	2043-2100	57
ssp119	IPSL-CM6A-LR	r14i1p1f1	2052	2004-2052	2052-2100	48
ssp119	IPSL-CM6A-LR	r1i1p1f1	2050	2000-2050	2050-2100	50
ssp119	IPSL-CM6A-LR	r2i1p1f1	2052	2004-2052	2052-2100	48
ssp119	IPSL-CM6A-LR	r3i1p1f1	2056	2012-2056	2056-2100	44
ssp119	IPSL-CM6A-LR	r4i1p1f1	2052	2004-2052	2052-2100	48
ssp119	IPSL-CM6A-LR	r6i1p1f1	2052	2004-2052	2052-2100	48
ssp119	MIROC-ES2L	r1i1p1f2	2047	1994-2047	2047-2100	53
ssp119	MIROC-ES2L	r2i1p1f2	2050	2000-2050	2050-2100	50
ssp119	MIROC-ES2L	r3i1p1f2	2048	1996-2048	2048-2100	52
ssp119	MIROC6	r1i1p1f1	2059	2018-2059	2059-2100	41
ssp119	MPI-ESM1-2-LR	r10i1p1f1	2049	1998-2049	2049-2100	51
ssp119	MPI-ESM1-2-LR	r11i1p1f1	2044	1988-2044	2044-2100	56
ssp119	MPI-ESM1-2-LR	r12i1p1f1	2052	2004-2052	2052-2100	48
ssp119	MPI-ESM1-2-LR	r13i1p1f1	2046	1992-2046	2046-2100	54
ssp119	MPI-ESM1-2-LR	r14i1p1f1	2047	1994-2047	2047-2100	53
ssp119	MPI-ESM1-2-LR	r15i1p1f1	2050	2000-2050	2050-2100	50
ssp119	MPI-ESM1-2-LR	r16i1p1f1	2054	2008-2054	2054-2100	46
ssp119	MPI-ESM1-2-LR	r17i1p1f1	2050	2000-2050	2050-2100	50
ssp119	MPI-ESM1-2-LR	r18i1p1f1	2051	2002-2051	2051-2100	49
ssp119	MPI-ESM1-2-LR	r19i1p1f1	2051	2002-2051	2051-2100	49
ssp119	MPI-ESM1-2-LR	r1i1p1f1	2047	1994-2047	2047-2100	53
ssp119	MPI-ESM1-2-LR	r20i1p1f1	2053	2006-2053	2053-2100	47
ssp119	MPI-ESM1-2-LR	r21i1p1f1	2044	1988-2044	2044-2100	56

ssp119	MPI-ESM1-2-LR	r22i1p1f1	2045	1990-2045	2045-2100	55
ssp119	MPI-ESM1-2-LR	r23i1p1f1	2038	1976-2038	2038-2100	62
ssp119	MPI-ESM1-2-LR	r24i1p1f1	2043	1986-2043	2043-2100	57
ssp119	MPI-ESM1-2-LR	r25i1p1f1	2052	2004-2052	2052-2100	48
ssp119	MPI-ESM1-2-LR	r26i1p1f1	2043	1986-2043	2043-2100	57
ssp119	MPI-ESM1-2-LR	r27i1p1f1	2056	2012-2056	2056-2100	44
ssp119	MPI-ESM1-2-LR	r28i1p1f1	2046	1992-2046	2046-2100	54
ssp119	MPI-ESM1-2-LR	r29i1p1f1	2050	2000-2050	2050-2100	50
ssp119	MPI-ESM1-2-LR	r2i1p1f1	2054	2008-2054	2054-2100	46
ssp119	MPI-ESM1-2-LR	r30i1p1f1	2047	1994-2047	2047-2100	53
ssp119	MPI-ESM1-2-LR	r3i1p1f1	2047	1994-2047	2047-2100	53
ssp119	MPI-ESM1-2-LR	r4i1p1f1	2043	1986-2043	2043-2100	57
ssp119	MPI-ESM1-2-LR	r5i1p1f1	2042	1984-2042	2042-2100	58
ssp119	MPI-ESM1-2-LR	r6i1p1f1	2046	1992-2046	2046-2100	54
ssp119	MPI-ESM1-2-LR	r7i1p1f1	2048	1996-2048	2048-2100	52
ssp119	MPI-ESM1-2-LR	r8i1p1f1	2048	1996-2048	2048-2100	52
ssp119	MPI-ESM1-2-LR	r9i1p1f1	2052	2004-2052	2052-2100	48
ssp119	MRI-ESM2-0	r1i1p1f1	2048	1996-2048	2048-2100	52
ssp534-over	ACCESS-ESM1-5	r1i1p1f1	2066	2032-2066	2066-2100	34
ssp534-over	CESM2-WACCM	r1i1p1f1	2068	2036-2068	2068-2100	32
ssp534-over	CESM2-WACCM	r5i1p1f1	2068	2036-2068	2068-2100	32
ssp534-over	CanESM5	r1i1p1f1	2072	2044-2072	2072-2100	28
ssp534-over	CanESM5	r2i1p1f1	2066	2032-2066	2066-2100	34
ssp534-over	CanESM5	r3i1p1f1	2068	2036-2068	2068-2100	32
ssp534-over	CanESM5	r4i1p1f1	2069	2038-2069	2069-2100	31
ssp534-over	CanESM5	r5i1p1f1	2068	2036-2068	2068-2100	32
ssp534-over	FGOALS-g3	r1i1p1f1	2054	2008-2054	2054-2100	46
ssp534-over	GISS-E2-1-G	r1i1p1f2	2060	2020-2060	2060-2100	40
ssp534-over	GISS-E2-1-G	r1i1p3f1	2063	2026-2063	2063-2100	37
ssp534-over	GISS-E2-1-G	r1i1p5f1	2064	2028-2064	2064-2100	36
ssp534-over	GISS-E2-1-G	r2i1p3f1	2062	2024-2062	2062-2100	38
ssp534-over	GISS-E2-1-G	r3i1p3f1	2064	2028-2064	2064-2100	36
ssp534-over	GISS-E2-1-G	r4i1p3f1	2062	2024-2062	2062-2100	38
ssp534-over	IPSL-CM6A-LR	r1i1p1f1	2072	2044-2072	2072-2100	28
ssp534-over	MIROC-ES2L	r1i1p1f2	2068	2036-2068	2068-2100	32
ssp534-over	MIROC6	r1i1p1f1	2063	2026-2063	2063-2100	37
ssp534-over	MRI-ESM2-0	r1i1p1f1	2062	2024-2062	2062-2100	38
ssp534-over	UKESM1-0-LL	r4i1p1f2	2072	2044-2072	2072-2100	28